# Maize *(Zea mays* L.) interaction with the arbuscular mycorrhizal fungus *Rhizophagus irregularis* allows mitigation of nitrogen deficiency stress: physiological and molecular characterization

**Authors** :

Bérengère Decouard[1], Niaz Bahar Chowdhury[2], Aurélien Saou[3], Martine Rigault[1], Isabelle Quilleré[1], Thomas Sapir[1], Anne Marmagne[1], Christine Paysant le Roux[4], Alexandra Launay-Avon[4], Florence Guerard[4], Caroline Mauve[4], Bertrand Gakière[4], Céline Lévy-Leduc[3], Pierre Barbillon[3], Rajib Saha [2], Pierre-Emmanuel Courty[5], Daniel Wipf[5], Bertrand Hirel[1], Alia Dellagi[1]*

1 : Université Paris-Saclay, INRAE, AgroParisTech, Institut Jean-Pierre Bourgin (IJPB), 78000, Versailles, France.

2 : Chemical and Biomolecular Engineering, University of Nebraska-Lincoln, Lincoln, NE, United States of America

3 : Université Paris-Saclay, AgroParisTech, INRAE, UMR MIA Paris-Saclay, 91120 Palaiseau, France

4 : Université Paris-Saclay, CNRS, INRAE, Université Evry, Institute of Plant Sciences Paris-Saclay (IPS2), 91190, Gif sur Yvette, France. Université Paris Cité, CNRS, INRAE, Institute of Plant Sciences Paris-Saclay (IPS2), 91190, Gif sur Yvette, France

5 : Agroécologie, AgroSup Dijon, Centre National de la Recherche Scientifique (CNRS), Université de Bourgogne, Institut National de Recherche pour l'Agriculture, l'Alimentation, et l'Environnement (INRAE), Université Bourgogne Franche-Comté, Dijon, France.

* Correspondance:

Prof. Alia Dellagi

Address: Université Paris-Saclay, INRAE, AgroParisTech, Institut Jean-Pierre Bourgin (IJPB), 78000, Versailles, France.

Phone: +33 1 30 83 32 28

E-mail: alia.dellagi@agroparistech.fr

Key words: N use efficiency; Nitrogen uptake; arbuscular mycorrhizal fungi, Maize, metabolic modelling.

**Abstract**

Maize is currently the most productive cereal crop in the world (www.faostat.org). It can associate with the Arbuscular Mycorrhizal Fungus (AMF) *Rhizophagus irregularis* which can provide additional water and mineral nutrients to the plant in return for C delivered by the host plant. Two maize lines were characterized at the physiological and molecular levels as they displayed contrasting responses to inoculation with the AMF when grown under optimal, medium, or low N fertilization conditions. For both these lines, the presence of the AMF allows development of a beneficial symbiotic association but only under limiting N fertilization conditions and allows to maintain plant biomass production when there is a five fold reduction in N supply. Physio-agronomical phenotyping and transcriptomic and metabolomic characterization of these two lines indicates that, (i) the level of N supply is the major factor affecting all studied traits; (ii) although the two lines display different transcriptomic and metabolomic responses to *R. irregularis* the agro-physiological traits are similar; and (iii) inoculation with the AMF relieves N deficiency stress. Analysis of the fungal transcriptome indicated that, like the plant transcriptome, it was also mainly affected by N nutrition level rather than by the maize host genotype. To explore potential metabolic pathways affected by the symbiosis, we integrated the transcriptomic data to model mycorrhized maize metabolism in a multi-organ Genome-scale metabolic model (GSM) *i*ZMA6517, based on a stoichiometric approach. Both maize transcriptomics data integrated *i*ZMA6517 model and *R. irregularis* transcriptome pointed to nucleotide and ureides metabolism as previously unexplored new drivers of the symbiotic N nutrition triggered by *R. irregu*laris that allow maize growth improvement.

## Introduction

Nitrogen (N) is the fourth most abundant component of plant biomass, which explains its pivotal role in agriculture (Hirel *et al.*, 2011; Hirel and Krapp, 2020). Indeed large inputs of N fertilizers are necessary to ensure optimal crop productivity (Hirel *et al.*, 2007, 2011). However, only 30 to 50% of the N available in the soil is taken up by most crops, resulting in important N losses which can cause damage to the environment such as water pollution and increased greenhouse effect (Schlesinger, 2009; Lassaletta *et al.*, 2016). It is urgent to minimize these impacts while simultaneously meeting the increasing demand for food production resulting from population growth. Ensuring crop productivity while minimizing N supply can be monitored by measuring nitrogen use efficiency (NUE). A better understanding of how to enhance NUE is a major challenge in the context of agroecology as it represents the capacity of the plant to produce grains or vegetative biomass per unit of available N (Hirel *et al.*, 2007; Lea and Miflin, 2018; Wang *et al.*, 2018; Liu *et al.*, 2022). Three physiological processes contribute to NUE: (Masclaux-Daubresse *et al.*, 2010; Lea and Miflin, 2018) : 1) N uptake efficiency involved in aquisition N from the soil by means of root-specific inorganic or organic N transporters (Fan *et al.*, 2017; Wang *et al.*, 2018); 2) N assimilation efficiency which is the incorporation of inorganic N into organic N-containing molecules necessary for plant growth and development (Hirel *et al.*, 2011; Hirel and Krapp, 2020; Wani *et al.*, 2021); and 3) N remobilization efficiency which represents the capacity of the plant to remobilize N and transfer it to storage organs (Masclaux-Daubresse *et al.*, 2010; Kant, 2018). To fulfil their N-associated metabolic needs, plants can establish symbiosis with beneficial soil microbes which help to improve their N nutrition by different mechanisms, some of which are well characterized. Exploiting the capacity of a crop to benefit from beneficial microbes in terms of N nutrition in order to maintain yields while reducing chemically synthesized N input is challenging in the context of a more sustainable agriculture (Gianinazzi *et al.*, 2010; Verzeaux *et al.*, 2017; Wipf *et al.*, 2019; Dellagi *et al.*, 2020; Gojon, 2022; Xie *et al.*, 2022).

The best characterized symbiosis which improves legume N nutrition occurs when symbiotic bacteria from the Rhizobiaceae family allows fixation of atmospheric $N_2$ and its reduction to $NH_4^+$ readily usable by the host plant (Udvardi and Poole, 2013; Masson-Boivin and Sachs, 2018). Nitrogen can also be transferred from the soil to the roots when the plant is colonized by Arbuscular Mycorrhizal Fungi (AMFs), a symbiotic process occurring in 80% of land plants including cereals (Gianinazzi *et al.*, 2010; Chen *et al.*, 2018*a*; Gojon, 2022; Xie *et al.*, 2022). AMFs are obligate biotrophs, meaning that they rely on their living host plants to complete their life cycle. The early steps of AMF symbiosis involve signal exchange between the host roots of the host plant and the fungus. This signalling process leads to establishment of a physical contact between the partners during which the fungus develops structures like a hyphopodium on the root epidermal cell followed by its growth inside these cells up to the cortical cells where it differentiates into highly branched structures called “arbuscules”. Around these arbuscules, the cortical cells undergo strong reorganization leading to the formation of a structure called “periarbuscular membrane” (PAM). Dual nutritional exchange occurs at the interface of this membrane where the transfer of carbon containing molecules derived from photosynthesis such as hexoses and lipids feed the fungus, which in turn provides minerals such as N and P (Smith and Read, 2002; Gianinazzi *et al.*, 2010; MacLean *et al.*, 2017; Choi *et al.*, 2018; Dellagi *et al.*, 2020). The extra-radical mycelium which represents an extension of the arbuscular structures, allows the fungus to explore the surrounding rhizosphere and to take up minerals further translocated to the periarbuscular interface to be finally delivered to the host plant. In many case, an AMF symbiotic association is able to increase tolerance to abiotic and biotic stresses (Choi *et al.*, 2018; Berger and Gutjahr, 2021).

It is well established that phosphorus (P) deficiency is the main driver for the establishment of mycorrhizal symbiotic associations (Breuillin *et al.*, 2010; Smith *et al.*, 2011; Balzergue *et al.*, 2013; Wang *et al.*, 2017; Paries and Gutjahr, 2023). Phosphorus deficiency triggers exudation from roots of signaling molecules such as strigolactones that stimulate AMF hyphal branching (Lanfranco *et al.*, 2018; Hull *et al.*, 2021). In addition, isotope tracing experiments have shown

that AMF provide phosphorus to their hosts (Sawers *et al.*, 2017; Das *et al.*, 2022). In contrast, the benefit of a mycorrhizal symbiosis in terms of N uptake and utilization by the host plant, remains to be fully characterized (Chen *et al.*, 2018*a*; Dellagi *et al.*, 2020; Gojon, 2022; Xie *et al.*, 2022). It is known that N can be transported to the plant by AMF (Courty *et al.*, 2015; Garcia *et al.*, 2016; Chen *et al.*, 2018*a*). Two transporters that mediate the mycorrhizal N transport pathway have been identified so far. For example, in rice, a transporter specifically involved in the transfer of nitrate to the roots of the host plant via the AMF has been described (Wang *et al.*, 2020). In maize, an ammonium transporter enabling the uptake of inorganic N has recently been characterised (Hui *et al.*, 2022).

Maize is currently the most productive cereal crop in the world (www.faostat.org) with a global yield exceeding that of rice (Liu *et al.*, 2020). Maize is grown for several purposes including animal feed, food and biotechnological applications (Ranum *et al.*, 2014; Revilla *et al.*, 2022). Different maize genotypes are able to develop a symbiotic association with AMF (Sawers *et al.*, 2018*a*; Berger and Gutjahr, 2021). Several studies have shown that AMF can supply substantial amount of N to maize (Quiroga *et al.*, 2020; Hui *et al.*, 2022). However, physiological and molecular characterization of maize's interaction with AMF under different N supply levels has never been undertaken. We reasoned that utilizing AMF to reduce N fertilization requires investigating the maize physiological responses to AMF under different levels of N fertilization. In the present study, we have studied in an integrated manner the impact of N nutrition on the interaction between maize and the AMF *Rhizophagus irregularis* both at the physiological and molecular levels. Using phenotyping, transcriptomic and metabolomic approaches, we have characterized such interaction using two maize lines which benefit from symbiotic association with the fungus in terms of agronomic performance. Genome-scale metabolic modeling (GSM) is a computational tool to model plant metabolism and can highlight potential key metabolic pathways in plant in response to environmental cues (Morris *et al.*, 2023). Initial efforts on maize metabolic models were limited to its leaf (Simons *et al.*, 2014) and root (Chowdhury *et al.*, 2022*b*) GSMs, which showed excellent agreement with existing literature regarding phenotypical predictions. Most recently, a multi-organ GSM

of maize line B73, *i*ZMA6517 (Chowdhury *et al.*, 2023), is proposed which includes full scale GSMs of root, stalk, kernel, and leaf; connected via phloem tissue. *i*ZMA6517 predicted organ-specific metabolic bottlenecks accurately and explored symbiotic relationship with *R. irregularis*. Thereby, apart from experimental works, we used *i*ZMA6517 to predict plant agronomic performance. Interestingly, *i*ZMA6517 identified purine and pyrimidine biosynthetic pathways as key physiological processes involved in the efficiency of N utilization in the symbiotic association.

## Material and methods

### Plant material, growth conditions and inoculation

The maize inbred lines used in this study B73 and Lo3 are described in Supplementary table 1. The reference maize genotype B73, for which the genome was fully sequenced, represents the reference genome for the maize species (Schnable *et al.*, 2009). Additionally, B73 is known be responsive to AMF, resulting in increased biomass (Ramírez-Flores *et al.*, 2019; Berger and Gutjahr, 2021). Lo3, was selected due to its enhanced biomass response following inoculation with *R. irregularis.* This selection was based on the outcomes of two rounds of screening aimed at identifying maize lines that exhibit increased biomass in the presence of AMF under limiting N conditions. These screening round were performed on the core collection previously described (Cañas *et al.*, 2017). The purpose was to identify maize genotypes which benefits from AMF inoculation (data not shown). The fungal strain used is the highest quality of purity strain *Rhizophagus irregularis* DAOM197198 (Agronutrition, Toulouse, France). Inoculum was prepared in distilled water and the required volume of spore suspension was added next to the germinated seed or plantlet with a pipette.

In all experiments, seeds were surface-sterilized as follows. Seeds were first incubated in ethanol for 5 minutes at 28°C followed by rinsing with distilled water. Then they were incubated for 45 minutes in a 15% commercial bleach solution with 0.01% Triton x100 then rinsed in distilled water. They were placed on wet sterile Whatman paper in Petri dishes closed with

parafilm and incubated in the dark for 48-72h at 20°C. Germinated seeds were selected and then sown in pots of 4 litres containing a mix of sterilized unfertilized peat (40% Baltic blond peat 0-10 mm, 60% Brown peat 0-10 mm, 75 g oligoelements, pH Cacl2 5.3 – 5.8, Stender, France) and dried clay beads (reference: 17831050 BILLE ARGILE LIA 8/16, Soufflet, France) 1:1/v:v. The experimental design and the different steps of growing and harvesting of the experiment in 2020 and 2021 are presented in Supplementary Figure 1 and 2 respectively. Meteorological conditions within the greenhouse during 2020 are depicted in Supplementary Figure 3. For each condition 9-10 plants were used. Three inoculations with spores of *R. irregularis* were performed as follow : The first inoculation with 500 spores/plant at sowing, second inoculation 1 week after sowing with 200 spores/plant and a third inoculation 2 weeks after sowing with 200 spores/plant. Control plants were treated with distilled water. Plants were grown under three different nitrogen regimes : low N (LN, 1mM $NO_3^-$), medium N (MN, 5 mM $NO_3^-$) and high N (HN, 10 mM $NO_3^-$). The specific composition of these regimes is provided in Supplementary Table 2. For each N regime, plants were irrigated for the first three weeks with the solution corresponding to the chosen N regime with low P (named P-) containing 10 µM phosphate in order to trigger AMF colonization. Then, at dates indicated in Supplementary Figure 1 and 2, irrigation was changed to the same N level but 300 µM P (named P+, Supplementary Table 2). Increasing P level in the irrigation solution was necessary to allow plants reach the maturity stage. To determine $^{15}N$ uptake, $^{15}N$ labelling was performed at indicated dates (Supplementary Figure 1). 100 mL of 45 mM $KNO_3$ solution enriched at 2% $^{15}N$ was applied to each plant in order to provide 1,25mg of $^{15}N$.

**Harvesting procedures**

Plants grown in 2020 were used for the phenotyping, metabolomics, RNA-seq and RT-qPCR experiments. Plants grown in 2021 were to monitor fungal colonization and RT-qPCR experiments. For RNA and metabolite extractions, leaf and root samples were harvested and frozen in liquid nitrogen before RNA extraction. Depending on the experiment and the biological question asked, one, two or three developmental stages were chosen for tissue

harvesting. Those stages were determined based a combination of two criteria: (i) the presence of arbuscular symbiotic structures in maize roots and (ii) plant developmental stages. The first one is the vegetative stage (VS) corresponding to the 7- to 8-leaf stage (Cañas *et al.*, 2017). This stage is an indicator of a highly metabolically and photosynthetically active leaf tissue but only few fungal structures start to be visible in roots. The second stage corresponds to 15 days after the Vessel Tasselling stage (VT+15 stage) where root colonization is clearly established and plant is in the early phase of flowering. This stage was chosen because it allows harvesting roots without imposing too great a stress on the plant in order to make sure kernels are not affected. The third stage is maturity stage (MS) and corresponds to plants displaying mature ears. Dates of harvesting for VS, VT+15 stage and MS differed depending on the condition and the year of experiment (Supplementary Figure 1 and 2). For leaf tissues, harvesting consisted in cutting a piece of 1 cm x 10 cm of leaf mesophyll along the midrib from the 6$^{th}$ fully emerged leaf for the VS. For VT+15 stage and MS, a piece of 1 cm x 10 cm leaf surface from the leaf below the ear of each individual plant was harvested. The leaf below the ear was chosen for providing a good proxy of the sink-to-source transition during grain filling (Prioul and Schwebel-Dugué, 1992).

Roots were harvested at VS, VT+15 stage or MS depending on the type of experiment. For each treatment/condition, roots were collected from 5 plants. Thin secondary roots were harvested from the surrounding root system, close to the pot borders. They were washed with distilled water, then frozen in liquid nitrogen or stored in distilled water. Following root harvesting, the plants grown in 2020 were left to grow until maturity. Thus, the roots used for the different omics analyses corresponded to the same plants as those that produced grains and were phenotyped for physio-agronomical traits.

**Quantification of yield, biomass, C, N, $^{15}$N and P**

Plant organs were harvested then oven dried at 80°C for 3 to 5 days then ground to fine powder. Yield was quantified by weighing dry grains. Biomass of the aerial parts including stalks, leaves, and cobs were weighed after drying. The upper regions of the root system was

harvested. This did not allow to quantify the whole root biomass since it was impossible but allowed to quantify the percentage of C, N and P. For each plant and each organ, 5,000 µg of dry powder was placed in tin capsules to quantify the total N and C concentrations using the FLASH 2000 Organic Elemental Analyzer (Thermo Fisher Scientific Villebon, France) and the $^{15}N$ enrichment using the Delta V Advantage isotope ratio mass spectrometer (Thermo Fisher Scientific, France). Supplementary Table 3 indicates the calculations of different traits with C and N content. A% (Atom percent) represents the $^{15}N$ enrichment in the sample [$^{15}N$/(total N)]. Since the natural $^{15}N$ abundance in N unlabeled samples was 0.3663 (A% control), specific enrichments due to the $^{15}N$ uptake were calculated as E% = (A% - 0.3363).The P concentration of shoots, grains and roots was measured using the molybdate blue method on a Shimadzu UV-160 spectrophotometer (Shimadzu Biotech) after acid digestion (Murphy and Riley, 1962).

**Quantification of root colonization level by AMF structures**

Thin secondary roots were harvested as indicated above and carefully washed in distilled water. They were incubated in 10% KOH overnight at room temperature. They were then rinsed in distilled water and incubated in 5% black ink (Sheaffer Skrip Bottled Ink, France) solution for 10 min at 70°C. Washing was performed by incubating roots in 8% acetic acid for 25 min. For the quantification of % of AM colonization (total, arbuscules, vesicles) 50 pieces of 1 cm length each were mounted on a slide for observation of AM structures under light microscope using the slide method (Giovannetti and Mosse, 1980). Quantifications were performed on roots collected from 5 plants for each condition.

**RNA extraction for RT qPCR and RNAseq**

RNA extraction was performed with TRIzol (Thermo Fisher Scientific, USA) protocol. Fresh tissue of leaves or roots (100 mg) were frozen in liquid nitrogen then ground to fine powder that was homogenized in 1 mL of TRIzol. Two glass beads are added to the extract in the tube which was then vortexed for 5 minutes, then the samples were incubated for 5 minutes at room temperature (RT). Two hundred microliters of chloroform were added then the sample was

vortexed for 5 minutes and incubated 3 minutes at RT. Samples are centrifuged at 12,000 g for 15 minutes at 4°C. The aqueous phase (approximately 500 µL) was transferred to a new tube with an equal volume of ethanol (100%). Samples mixed with ethanol were then transferred to a column (Zymo-Spin™ IC, Germany); for purification following manufacturer's instructions.

**cDNA synthesis and RT-PCR**

1 µg of RNA was first treated with DNAse (Thermo Fisher Scientific, USA) in a 10 µL total volume. 1 µg of DNAse treated RNA was then used for reverse transcription using oligo-dT and the reverse trancriptase Revert aid (Thermo Fisher Scientific, USA) following the manufacturer's instructions. Quantitative PCR reactions were carried out as described (Verly *et al.*, 2020). For each sample, a cycle threshold (Ct) value was determined and converted into Starting Quantity (SQ) also named Arbitrary Units (AU) values based on a standard curve equation. The AU values obtained for each gene of interest was then divided by the mean of AU values obtained for the chosen reference gene (indicated in each dataset) leading to the normalized transcript level value. Primer sequences are described in Supplementary table 4.

**RNAseq and Bioinformatic Analysis**

RNA-seq libraries were constructed by the POPS platform (IPS2) using the Illumina Stranded mRNA Prep kit (Illumina®, California, U.S.A.) according to the supplier's instructions. Libraries were sequenced by the Genoscope (Évry-Courcouronnes, France) on a Novaseq 6000 instrument (Illumina) with 150 base paired-end sequences.

***Raw Data cleaning***

The raw data were treated as follow:

1- Illumina filter. Performed as described with chastity cutoff of 0,6.

To remove the least reliable data from the analysis, the raw data were filtered to remove any clusters that have "too much" intensity corresponding to bases other than the called base. The purity of the signal from each cluster was examined over the first 25 cycles and calculated as Chastity = Highest_Intensity / (Highest_Intensity + Next_Highest_Intensity) for each cycle. The default filtering implemented at the base calling stage allows at most one cycle that is less than the Chastity threshold (0,6).

2- Genoscope filter. An in-house procedure was used in order to remove adapters and primers on the whole read and low-quality nucleotides from both ends (while quality value is lower than 20) and then continue next steps with the longest sequence without adapters and low-quality bases. Remove sequences between the second unknown nucleotide (N) and the end of the read. This step is done on trimmed (adapters + quality) reads. Discard reads shorter than 30 nucleotides after trimming. Remove read pairs that come from the low-concentration spike-in library of Illumina PhiX Control. Reads pairs corresponding to ribosomal RNA were removed using sortMeRNA (v2.1, (Kopylova *et al.*, 2012).

These previous two steps were performed by the sequencing facility at Genoscope. Cleaned reads from Genoscope were adapter trimmed again by the POPS platform with BBduk from the BBmap suite (v38.84, Bushnell, 2014) with the options k=23 ktrim=r qtrim=r useshortkmers=t mink=11 trimq=20 hdist=1 tpe tbo minlen=30 using adapter sequences file included in the BBTools package.

*Mapping and Gene expression quantification*

Filtered reads were then mapped and counted using STAR (v2.7.3a, (Dobin *et al.*, 2013)) with the following parameters --alignIntronMin 5 --alignIntronMax 60000 --outSAMprimaryFlag AllBestScore --outFilterMultimapScoreRange 0 --outFilterMultimapNmax 20 on a combined reference genome made by concatenating the files of the *Zea mays* B73 (V4.49) and *Rhizophagus irregularis* (V2) reference genomes and the associated GTF annotation files

(also combined). Between 75.3 and 96.1 % of the reads were uniquely mapped (median = 91.9%). Between 68 and 88 % of the reads were associated to annotated genes (median = 85.3%).

Statistical Analyses of Expression Data

Statistical analyses were conducted on R v3.6.2 (R Core Team, 2020) using the script-based tool DiCoExpress (Lambert *et al.*, 2020; AU - Baudry *et al.*, 2022). DiCoexpress used the Bioconductor package edgeR (v 3.28.0, (Robinson *et al.*, 2010; McCarthy *et al.*, 2012).The raw count file used for the statistical analyses only contain the reads of the *Zea mays* organism. Dicoexpress DiCoExpress analyse RNAseq projects with at most two biological factors. For this reason and to answer biological questions of interest, 4 separate statistical analyses were conducted on samples from (I) B73 leaves, (ii) B73 roots, (iii) Lo3 leaves, (iv) Lo3 roots.

Gene Filtering and Normalization

For the four analyses, low counts genes giving low counts were filtered using the "FilterByExpression" feature available through the edgeR package with a minimum count threshold of 15. Raw counts were normalized with the trimmed mean of M values (TMM) method implemented in edgeR package.

*Differential Expression Analysis*

The differential analysis is based on a negative binomial generalized linear model. For the 4 *Zea mays* analyses, the log2 of the average normalized gene expression is an additive function of a condition effect (LN or HN), a treatment effect (Ri or Ctrl), an interaction between the condition and the treatment and the technical replicate factor (3 modalities). To make the processing of these multifactorial designs easier, Differential Expression (DE) analyses were performed using the DiffAnalysis_edgeR function of DiCoExpress to generate automatically the contrasts. In each analysis, we considered the difference between the two treatments at each condition and averaged on the two conditions, the difference between the two conditions given a treatment and averaged on the two treatments and the interaction effect defined as the

difference between the two treatments at a given condition (HN) minus the difference between the two treatments at the second condition (LN). It leads to a total of 8 contrasts per analysis and only biologically meaningful contrasts were interpreted. For each contrast a likelihood ratio test was applied and raw p-values were adjusted with the Benjamini–Hochberg procedure to control the false discovery rate. The distribution of the resulting p-values followed the quality criterion described by Rigaill et al. (Rigaill *et al.*, 2018). A gene was declared differentially expressed if its adjusted p-value was lower than 0.05.

For the fungal transcripts, expression ratios were considered relative to the N nutrition condition. Fungal transcripts displaying a FC higher or lower than 1.5 in LN compared to HN conditions were considered Each transcript ID was converted into the protein ID using the fungal genomic resource Mycocosm at the JGI website: https://mycocosm.jgi.doe.gov/pages/search-for-genes.jsf?organism=Rhiir2_1 (Tisserant *et al.*, 2013; Chen *et al.*, 2018*b*). Based on KOG (euKaryotic Orthologous Groups), functional classes to which the genes belong were determined Over-represented functional KOG categories of these fungal genes were determined using the 'KOGMWU' 1.2 R package (Date 2019-02-19. Author Mikhail V. Matz). The fold enrichment value is based on a Mann-Witney, U-test that uses for each gene, a combination of the FC and the KOG category.

**Metabolomic analyses**

All extraction steps were performed in 2 mL Safelock Eppendorf tubes. The ground dried samples (5 mg DW) were resuspended in 1 mL of frozen (-20°C) Water:Acetonitrile:Isopropanol (2:3:3) containing Ribitol at 4 mg/L and extracted for 10 min at 4°C with shaking at 1500 rpm in an Eppendorf Thermomixer. Insoluble material was removed by centrifugation at 13500 rpm for 10 min. 700 µL were collected and 70 µL of myristic acid d27 at 0.3 g/L was added as an internal standard for retention time locking. After centrifugation, aliquots of each extract (100 µL) were dried for 4 h at 35 °C in a Speed-Vac and stored at -80°C. Two Blank tubes underwent the same steps as the samples.

Sample derivatization and analysis : All steps of GC-MS analyses were done as described in Fiehn et al. (Fiehn, 2006; Fiehn *et al.*, 2008). Agilent literature PUB: 5989-8310EN (Agilent G1676AA Agilent Fiehn GC/MS Metabolomics RTL Library User Guide. June 2008. Agilent P/N: G1676-90000, Agilent Fiehn GC/MS Metabolomics RTL Library Product Note. May 2008). Samples were taken out of -80°C, warmed 15 min before opening and speed-vac dried again for 1 hour at 35 °C before adding 10 µl of 20 mg/mL methoxyamine in pyridine to the samples and the reaction was performed for 90 min at 30°C under continuous shaking in an Eppendorf thermomixer. 90 µL of N-methyl-N-trimethylsilyl-trifluoroacetamide (MSTFA) (REGIS TECHNOLOGIES 1-270590-200 -10x1g) were then added and the reaction continued for 30 min at 37°C. After cooling, 90 µL were transferred to an Agilent vial for injection.

4 hours after derivatization 1 µL of sample was injected in splitless mode on an Agilent 7890B gas chromatograph coupled to an Agilent 5977A mass spectrometer. The column was an ZORBAX DB5-MS from Agilent (30 m with 10 m integraguard column - ref 122-5532G). An injection in split mode with a ratio of 1:30 was systematically performed for saturated quantification compounds. Oven temperature ramp was 60 °C for 1 min then 10 °C/min to 325 °C for 10 min. Helium constant flow was 1.1 mL/min. Temperatures were as follows: injector: 250°C, transfer line: 290°C, source: 230 °C and quadripole 150 °C. The quadrupole mass spectrometer was switched on after a 5.90 min solvent delay time, scanning from 50-600 µ. Absolute retention times were locked to the internal standard d27-myristic acid using the RTL system provided in Agilent's Masshunter software. Retention time locking reduces run-to-run retention time variation. Samples were randomized. A fatty acid methyl esters mix (C8, C9, C10, C12, C14, C16, C18, C20, C22, C24, C26, C28, C30) was injected in the middle of the queue for external RI calibration.

Data processing and quantification: Raw Agilent datafiles were analyzed with AMDIS http://chemdata.nist.gov/mass-spc/amdis/. The Agilent Fiehn GC/MS Metabolomics RTL Library (version June 2008) was employed for metabolite identifications. This library is the most comprehensive library of metabolite GC/MS spectra that is commercially available. It contains

searchable GC/MS EI spectra and retention time indexes from approximately 700 common metabolites. Peak areas determined with the Masshunter Quantitative Analysis (Agilent) in splitless and split 30 modes. Because automated peak integration was occasionally erroneous, integration was verified manually for each compound in all analyses. Resulting areas were compiled in one single Excel file for comparison. Peak areas were normalized to Ribitol and Dry Weight. Metabolite contents are expressed in arbitrary units (semi-quantitative determination).

**Amino acid quantification by OPA-HPLC**

Extraction procedure was identical that one described for metabolomics. Here 200µL of the extraction solution was taken and dried in a Speed-Vac evaporator for 2 h at 30°C before adding 1,3 mL of $H_20$ milliQ. The o-phtaldialdéhyde (OPA) reagent was made 48 h before first use by dissolving OPA at 12mg/mL in 200 µL of methanol and adding 1.8 mL of sodium borate 0.5M (pH 9.5) and 40 µL of 2-mercaptoethanol. The reagent was filtered into an autosampler vial and used for up to 3 days. Precolumn derivatization was performed in the injection loop by automated mixing of 10 µL sample and 10 µL OPA reagent, followed by a delay of 2 min prior to injection. The HPLC (Alliance Waters 2695, Waters Corporation, Massachusetts, USA) fitted with a fluo detector (Multi λ Fluorescence Detector 2475) was used. Compounds were measured at λ excitation of 340 nm and λ emission of 455 nm. The chromatographic separation was performed with Symmetry C18 column (3.5µm, 4.6*150 mm) by gradient elution at 40 °C using buffer A (20% methanol, 80% sodium acetate, 1% tetrahydrofuran, pH 5.9) and buffer B (80% methanol, 20% sodium acetate, pH 5.9). Buffer flow rate was 0.8 mL/min throughout and total run time per injection was 42 min. The chromatography data were analysed by Empower software. Peak identity was confirmed by co-elution with authentic standards. Concentration was calculated with calibration curve using peak area of compound of interest.

**Statistical analyses**

All statistical analyses were performed with RStudio 2023.06.0+421 "Mountain Hydrangea" under the free software environment R version 4.3.1 (Beagle Scouts). All Anova were implemented with the “aov” R package. All heatmaps were generated with the estimated marginal means that were calculated using the R package “emmeans”. Heatmap for physio-agronomical traits was generated with ‘pheatmap’ 1.0.12 package (Date 2019-01-04. Author Raivo Kolde) by implementing the ward.D2 hierarchical clustering method (Murtagh and Legendre, 2014). Heatmap for physio-agronomical traits was generated with the ‘pheatmap’ R package 1.0.12 Date 2019-01-04 (Author Raivo Kolde). Heatmaps for metabolomics, including the interactive ones, were generated with “heatmaply” R package (Galili *et al.*, 2018)

Metabolomics data were analyzed with the R package MultiVarSel (Perrot-Dockès *et al.*, 2018) which is the implementation of the variable selection approach in the multivariate linear model proposed in (Perrot-Dockès et al., 2018a), theoretically analysed in (Perrot-Dockès et al., 2018b) and applied in several contexts of omics data analyses such as (Grandclaudon *et al.*, 2019; Perrot-Dockès *et al.*, 2022). Using a joint clustering method based on a multipartite stochastic block model (Bar-Hen *et al.*, 2022) implemented in the R package sbm. The list of R packages used in this study: Chiquet J, Donnet S, Barbillon P (2023). *sbm: Stochastic Blockmodels*. R package version 0.4.5-9000, <https://grosssbm.github.io/sbm/>. Kolde R (2019). _pheatmap: Pretty Heatmaps_. R package version 1.0.12, <https://CRAN.R-project.org/package=pheatmap>. Lenth R (2023). _emmeans: Estimated Marginal Means, aka Least-Squares Means_. R package version 1.8.6, <https://CRAN.R-project.org/package=emmeans>. Perrot-Dockès M, Lévy-Leduc C, Chiquet J. R package MultiVarSel available from the Comprehensive R Archive Network, 2017. <https://CRAN.R-project.org/package=MultiVarSel>.

**Genome-Scale Metabolic Modelling (GSM) and Transcriptomics Data Integration**

To investigate the metabolism of maize from systems level, we used *i*ZMA6517 as the template model(Chowdhury *et al.*, 2023). The model is specific to B73 genotype and consists of organ-specific GSMs of root, stalk, leaf, and kernel. All these individual organ GSMs are connected

through a common phloem pool. The model has been described (Chowdhury *et al.*, 2023). The model was contextualized with HN Control, HN Rhizo, LN Control, and LN Rhizo using EXTREAM algorithm (Chowdhury *et al.*, 2023). The upper and lower bounds for the mentioned conditions are presented in the Supplementary Table 5. The General Algebraic Modeling System (GAMS) version 24.7.4 with IBM CPLEX solver was used to run FBA and FVA, E-Flux, and the FSA algorithm on the model. Each of the algorithms was scripted in GAMS and then run on a Linux-based high-performance cluster computing system at the University of Nebraska-Lincoln. Instructions for running files in GAMS through NEOS server have been published (Chowdhury *et al.*, 2022*a*). All the necessary files for COBRApy users can also be accessed through the *i*ZMA6517 publication (Chowdhury *et al.*, 2023).

**Metabolic Bottleneck Analysis (MBA)**

To determine the metabolic bottlenecks in each of HN Control, HN Rhizo, LN Control, and LN Rhizo conditions, we used Metabolic Bottleneck Analysis **(**MBA) (Chowdhury *et al.*, 2023). MBA expands the flux space of each reaction separately and assesses its impact on the whole plant biomass growth rate. Further details on MBA can be accessed in the original publications. MBA pinpoints plant-wide metabolic bottlenecks, which were further analyzed for biological insights.

## Results

### The impact of *Rhizophagus irregularis* on maize growth and yield is strongly dependent on the level of N nutrition

To investigate the molecular and physiological mechanisms involved in maize interaction with AMF in terms of N nutrition and have an overview of the diversity of these mechanisms we used two AMF-responsive maize lines B73 and Lo3. In order to find at which level of N fertilization the two lines benefit most from the fungal inoculation, these were grown in a greenhouse under low N (LN), medium N (MN) or high N (HN) corresponding to 1 mM $NO_3^-$, 5 mM $NO_3^-$ and 10 mM $NO_3^-$ in the nutrient solution respectively. The impact of *R. irregularis*

inoculation on maize physio-agronomic traits was monitored by measuring shoot biomass, grain yield, total N content and $^{15}N$ enrichment allowing the calculation of other traits such as NUE as described in Supplementary table 3. In inoculated plants, an increase in the shoot biomass production was only observed under LN in both lines, whereas an increase in grain yield only occurred in B73 (Figure 1A, 1B). A slight negative impact of *R. irregularis* inoculation was observed on B73 grain yield when plants were grown under HN. Interestingly, *R. irregularis* allowed inoculated plants grown under LN to produce a similar vegetative biomass compared to non-inoculated plants fed with 5 times more $NO_3^-$. However, AMF inoculation did not influence shoot biomass of either maize genotypes under MN or HN (Figure 1B).

In inoculated plants, an increase in NUE for grain was observed under LN and MN fertilization conditions only in B73 (Figure 1D). Aerial parts NUE increased only in LN conditions for both B73 and Lo3 (Figure 1C). Together, these data indicate that benefit from AMF in terms of maize yield and NUE is higher under limiting N supply than under ample N supply and depends on the genotype. When we examined the impact of the AMF on N resource allocation under the three levels of N, a significant increase of biomass allocation to the grain was observed in both B73 and Lo3 only in LN (Figure 1E**)**. Chlorophyll quantities were monitored during the vegetative phase and were also increased by AMF inoculation under LN only (Figure 1F).

The grain N content, considered as a proportion relative to dry mass, remains consistent across genotype and the N feeding conditions. However, an exception to this trend is observed in the B73 genotype, where the N content is notably lower in inoculated LN and MN plants (Figure 2A). Both the shoot and the root N contents were roughly proportional to the amount of N provided to the plant. Fungal inoculation did not change N content under LN. However, under higher N supply levels, a significant increase in the N content of aerial parts was observed in response to *R. irregularis* under MN for B73 and under HN for Lo3 indicating that these lines are able to store higher levels of N in the vegetative parts upon association with the AMF even under ample N (Figure 2C). The C/N ratio exhibited minimal change, as a slight decrease in B73 inoculated LN plants aerial parts and increase in grains in response to *R.*

*irregularis* under MN for B73 was observed (Figure 2G-H). Changes in carbon (C) content were not statistically significant.

To determine whether N uptake is modified during the symbiotic interaction, plants were labelled with a pulse of $^{15}N$ provided at the vegetative stage. The total quantity of $^{15}N$ in aerial parts and grains measured at maturity is unchanged whatever the treatment (Supplementary Figure 4). These data indicate that the fungus does not affect N uptake at the vegetative stage. However, under LN conditions, $^{15}N$-enrichment in the different organs of the inoculated plants was much lower than in control plants for both B73 and Lo3 in line with a biomass increase resulting in $^{15}N$ dilution in AMF inoculated plants (Supplementary Figure 4). These data indicate that the higher uptake of N triggered by *R. irregularis* is more likely to occur after the vegetative stage.

It is well established that mycorrhizae play a pivotal role in the improvement of plant P nutrition and uptake (Choi *et al.*, 2018; Plassard *et al.*, 2019; Paries and Gutjahr, 2023). To determine if the amount of N supplied to the plant and the presence of *R. irregularis* modify B73 and Lo3 phosphate content, total P content (TPC) was measured by the molybdate blue method. In inoculated plants, an increase in the TPC content was observed under HN conditions both in the grains and in the roots of Lo3, whereas for B73 it was in the shoots and in the roots under HN (Figure 2B-D-F). Together, these data indicate that N supply has a strong impact on mycorrhiza-mediated P nutrition and that this benefit depends on maize genotype.

**Inoculation by *R. irregularis* mitigate the physiological impact of N-deficiency**

Physio-agronomic phenotyping prompted us to determine if there were traits that could discriminate inoculated and non-inoculated plants. For this purpose, hierarchical clustering analysis (HCA) was performed using the physio-agronomic traits listed in Supplementary Table 3. The HCA presented in Figure 3. shows that the N supply, the genotype, and the symbiotic association had an impact on the monitored traits. All the LN plants were grouped in cluster A. Within cluster A, values for the traits related to N and P uptake, N uptake efficiency and $^{15}N$

enrichment including R_Ppercent, AP_Ppercent, AP_NUE, AP_15NEpercent, R_15NEpercent were higher. LN plants in cluster A were distant from the HN MN plants clustered in group B. In cluster B, genotypes were distributed into two subgroups, B1 and B2. Traits related to yield and biomass were grouped in cluster B irrespective of the inoculation status. Interestingly, in cluster A, traits related to N deficiency exhibited higher values in the control compared to the inoculated plants indicating that *R. irregularis* allowed plants to behave more similarly to group B plants, albeit still under N stress deficiency. These data show that *R. irregularis* inoculation can mitigate the impact of N limitation on physio-agronomic traits.

**Marker genes for N uptake and assimilation are differentially regulated in response to AMF inoculation and N supply**

The finding that several NUE traits, notably those related to $NO_3^-$ uptake were modified by AMF treatment prompted us to investigate further which molecular components were involved. Before investigating in details, the molecular mechanisms taking place in regard to on N supply we had to identify the time point of the interaction process at which symbiotic markers were expressed at their maximum. For this purpose, the expression level of symbiotic marker genes was monitored at three stages determined (see materials and methods). Then, the level of transcripts for the plant genes *ZmAMT3.1*, *ZmPHT6.1* and *ZmNPF4.5* markers of the symbiotic association and representative of $NH_4^+$, phosphorus and $NO_3^-$ transport respectively was quantified (Sawers *et al.*, 2017; Wang *et al.*, 2020; Xie *et al.*, 2022; Hui *et al.*, 2022). For the three genes, root transcripts were mostly more abundant at VT+15 stage in both HN and LN conditions (Supplementary Figure 5). Fungal colonization was greater under HN compared to LN both in B73 and Lo3 (Supplementary Figure 5A). The VT+15 stage was thus selected for all subsequent experiments.

The expression of selected marker genes involved in direct N transport, P and N transport mediated by AMF was then monitored in roots following inoculation by the AMF and according to the level of N supply. By monitoring the level of *R. irregularis* constitutive transcript *RiLSU* we confirmed that high N input led to increased fungal biomass in roots (Figure 4B). The

expression level of the four well known symbiotic markers mentioned before, *ZmPHT1.6*, *ZmNPF4.5*, *ZmHA1*, a proton pump, and *ZmAMT3.1* (Wang *et al.*, 2014, 2020; Sawers *et al.*, 2017; Xie *et al.*, 2022; Hui *et al.*, 2022), appears to be in general unregulated in response to the fungus in both genotypes and under all N supply conditions. It is interesting to notice that the higher the N nutrition level, the higher the expression of these markers (Figure 4A). To know more about direct transport and N assimilation genes in those conditions, we investigated expression levels of two maker genes of N starvation stress *(ZmNRT2.1a, and ZmNRT2.2)* encoding high affinity transporters, known to be upregulated under N deficiency (Krapp *et al.*, 2014; Wang *et al.*, 2018; Dechorgnat *et al.*, 2019; Hirel and Krapp, 2020) (Figure 4A). As expected, the level of N supply had a drastic effect in both maize genotypes on transcripts levels for the nitrate transporters *ZmNRT2.1a, ZmNRT2.2* which were more highly expressed in LN plants compared to MN and HN plants. These data indicate that the presence of the fungus mimics an additional N supply.

**Leaf and root transcriptome reprogramming in response to *R. irregularis* colonization integrates both a genotype and an N- availability effects**

To deepen the characterization of the biological processes involved in maize response to *R. irregularis* colonization as a function of N fertilization, a whole genome transcriptomic approach was conducted in leaves and roots of plants grown under HN and LN conditions. For this purpose, ddifferentially expressed genes (DEGs) exhibiting a fold change higher than 1.5 ($p$<0.05) in inoculated plants compared to non-inoculated plants were considered. It is important to note that RNAs used for the transcriptomic approach were obtained from the same plants that were phenotyped at the end of their life cycle for physio-agronomical traits. Indeed, root harvesting for molecular studies was not destructive, allowing plants to complete their life cycle.

Details for the numbers of DEGs depending on organ, N nutrition level and genotype are shown in Supplementary Figure 6. First, we focused on the DEGs in roots and in leaves irrespective of the genotype and irrespective of the level of N fertilization. In leaves, only 2 genes were up

regulated and only 2 genes were down regulated, whereas in roots many more genes were differentially expressed in all conditions in response to the fungus. The two genes up regulated in all conditions in leaves encode a H(+)-exporting diphosphatase (Zm00001d015569) involved in vacuole ion transport and a Histidine-containing phosphotransferase protein 4 (Zm00001d043505) involved in signalling. The two down regulated genes encode a Mannan endo-1,4-beta-mannosidase (Zm00001d010039) involved in cell wall remodelling and a Nuclear transcription factor Y subunit (NF-Y) (Zm00001d006835).

When considering root DEG genes irrespective of the genotype or N supply, there was an increase in the expression level of 345 genes whereas a decease was observed for 59 genes (Supplementary Figure 6). GO enrichment analysis revealed that for those common up-regulated genes in roots, the biological processes overrepresented were those related to proteolysis inhibition, lipid metabolism, ethylene response and membrane transport. The common down regulated genes were represented by five main functional categories including cell wall biogenesis, metal homeostasis, phosphate transport, stress responses and lipid metabolism (Figure 5).

To gain insight into the specific mechanisms taking place in each line (B73 and Lo3) upon symbiotic association as a function of N nutrition, enriched GO functions in DEG under LN or HN in each organ were determined. In response B73 roots under LN, main overrepresented categories of up-regulated transcripts are related to plant immunity represented by hormone signaling and phenylpropanoid pathway, cell wall remodeling and nucleotide metabolism, while the main down-regulated categories were enriched in post translational modifications such as histone de-ubiquitination. In B73 roots under HN, the main overrepresented categories in up-regulated genes are related to defense, signaling, glycolysis, lipid metabolism and cellular trafficking while the overrepresented categories in the down-regulated genes are related to sugar and steroid metabolism, cell division.

In inoculated Lo3 roots, under LN, stress responses, amino acid biosynthesis and autophagy are overrepresented in the up-regulated genes, while in the down-regulated genes, DNA and

amino acid metabolism as well as cell wall remodeling are overrepresented. Under HN, *R. irregularis* inoculation of Lo3 triggers the up-regulation of root transcripts mainly related to photosynthesis, stress responses, DNA metabolism, water transport, amino-acid metabolism, root development and terpenoid biosynthesis. In roots of HN grown Lo3 plants, the main overrepresented categories of down-regulated genes belong to nitrate assimilation, oligopeptide transport and stress responses categories.

We performed the same data analysis in leaves (Figure 5). In response to *R. irregularis*, the B73 leaves main overrepresented categories of up-regulated transcripts under LN conditions are related to translation and auxin signaling, while the main down-regulated categories were enriched in symbiotic interactions, signaling. Under HN, in B73 leaves of inoculated plants, the main overrepresented categories in up-regulated genes are related to redox reactions, carbohydrate transport and defense while the main over-represented categories in the down-regulated genes are related to protein folding and response to inorganic substances.

In leaves of inoculated Lo3 plants, under LN, the main overrepresented categories in the up-regulated genes are photosynthesis, cell wall remodeling, cytoskeleton remodeling, stress response, signaling, while in the down-regulated genes, gamma-amino butyric acid (GABA) metabolism and pyrimidine biosynthesis are overrepresented. Under HN, *R. irregularis* inoculation of Lo3 plants triggers the up-regulation of leaf transcripts mainly related to amino acid catabolism, flavin-containing compounds related metabolism and organic acid transport as well as iron homeostasis, while down-regulated genes belong to lipid metabolism, pyrimidine metabolism, and stress response. Taken together, these data show that leaf and root transcriptomic responses to the AMF differ depending on maize genotype and N supply.

**Leaf and root metabolomic profiles in response to *R. irregularis* are shaped by N nutrition**

To further characterize the metabolic responses of the two maize lines to *R. irregularis* inoculation, a primary metabolome profiling was performed on the same leaf and root samples

as those studied in the previous section. Metabolic profiles showed that plant organ and N supply had the strongest impact on leaf and root metabolite composition (Supplementary Figures 7A and B). AMF inoculation and maize genotype had globally weaker impacts on metabolite profiles (Figures 6 A and B and supplementary Figure 7C and D). In leaf samples 132 water soluble metabolites were detected of which 103 were significantly different after ANOVA statistical analysis ($P < 0.05$) followed by a Bonferroni post-hoc test and correction, in at least on condition. In roots, there were 120 water-soluble metabolites of which 117 were found to be significantly different in at least one condition with the same statistical analysis as above. The identity of metabolites can be found on the interactive heatmap Supplemantary interactive File 1.

In roots, fungal inoculation triggered accumulation of lipids such as trans-13-octadecenoic acid and palmitoleic in both lines Supplementary Figure 8. The accumulation of these two lipids was much higher under HN than under LN. We observed that in inoculated roots, there was a global decrease in sucrose, glucose and fructose levels in roots of Lo3 under LN. Several metabolites linked to N metabolism were differentially accumulated in inoculated roots. For example, Glu, Arg, citrulline, Asn and β-Ala levels were increased in response to *R. irregulari*s in roots under HN. Glutamine levels remained unchanged in inoculated roots. Some metabolites related to immunity were accumulated differentially in response to the fungus. For instance, shikimic acid was accumulated in LN roots of inoculated B73 plants and trehalose was accumulated in HN inoculated roots of both lines compared to controls.

In leaves, lipids and soluble sugars (glucose and fructose) did not show differential accumulation in response to the fungus. Sucrose, however, showed a significant decrease only for HN and this in both lines (Supplementary Figure 9). Gln and Asn accumulated in Lo3 leaves under HN in response to *R. irregularis*. Xylulose accumulated in Lo3 R LN leaves.

To identify metabolites representative of the plant response to *R. irregularis* under each growth condition, metabolites for which abundance is significantly correlated with specific treatment conditions were identified thanks to a variable selection approach in a multivariate linear model

conducted with the MultiVarSel approach (Figure 6 C and D). For example, we found that under LN, xylulose was accumulated in leaves of Lo3 inoculated plants (Figure 6C). In roots, benzoic acid was accumulated in inoculated B73 roots of plants grown under LN (Figure 6D). Palmitoleic acid is down accumulated in Lo3 HN control conditions compared to all the other conditiions. These data indicate that specific metabolites are accumulated depending on the plant genotype and the N supply in response to *R. irregularis*.

Using a joint clustering method (see material and methods), we analysed the links between the transcriptomic, metabolomic and physiological datasets and the experimental groups (Supplementary table 6, Figure 7). In roots, this analysis enabled us to identify 2 experimental groups (E1, E2), 3 transcript groups (t1, t2, t3), 2 metabolites groups (M1, M2) and 1 physiological trait group (P1). The different physiological traits do not exhibit strong contrasts in their expression to be separated into distinct groups. They are strongly associated associated with experimental group 1 (E1), which primarily consists of plants under HN and control, it means that these physiological traits take higher values in (E1) than in (E2) which are composed mostly of plants under LN conditions and enriched in inoculated plants. The metabolites identified in M1 are primarily associated with (E2) consisting mainly of inoculated plants and could be interpreted as a consequence of the inoculation. These results are consistent with the analysis conducted with the MultiVarSel approach highlighting the correlation between inoculated condition and the accumulation of, for example, glutamine, tyrosine or benzoic acid (Figure 6). Some of the transcriptomic data exhibit only weak correlations with both experimental groups (t3) as the second group of metabolites (M2). Experimental groups 1 and 2 also show strong correlations with t1 and t2 is only correlated with E1 (Figure 7). In leaves, this analysis only revealed that the two experimental groups represent a genotype, Lo3 or B73 (data not shown). Further analysis is required to elucidate the complex links between these data sets and experimental conditions.

**Multi-organ metabolic modelling reveals key metabolic processes triggered by *R. irregularis* allowing maize to mitigate N limitation stress**

To identify key metabolic reactions involved in yield and biomass reshaping in response to *R. irregularis* symbiosis, we integrated the transcriptomic data in a recently reconstructed multi-organ genome scale modelling (GSM) named *i*ZMA6517 (Chowdhury *et al.*, 2023), This model was built for the B73 maize genotype using the transcriptomic data integration algorithm, EXTREAM (Chowdhury *et al.*, 2023), followed by a metabolic bottleneck analysis (MBA) to pinpoint metabolic bottlenecks for biomass production. The B73 leaf and root transcriptomic data were used as input to EXTREAM to contextualized *i*ZMA6517. The modelling predicted that growth rates were higher under LN in response to *R. irregularis* inoculation which resulted in grain yield and biomass increase while under HN, a negative impact on maize growth rate was observed (Figure 8A). Strikingly, these data are in agreement with the observed yield and biomass experimental data in Figure 1, confirming the accurate phenotypic prediction of the *i*ZMA6517. This result prompted us to determine the metabolic processes that could explain the improved yield under LN B73 plants in response to *R. irregularis* inoculation by identifying the metabolic bottlenecks relieved by the AMF under limiting N. For this purpose, we compared the bottlenecks identified in LN control plants to the bottlenecks identified in inoculated LN plants (Figure 8B; Table 1). Four metabolic bottlenecks relieved by *R. irregularis* inoculation were identified; photosynthesis, purine and pyrimidine metabolism, aromatic acid metabolism; and folate metabolism (Figure 8B, Table 1). Interestingly 13 new bottlenecks were emerged following *R. irregularis* inoculation. These new bottlenecks are involved in the metabolism of purine, nicotinate, nicotinamide, purine, aromatic amino acids, Calvin cycle and glycolysis, On the other hand, we found that in HN plants, four metabolic bottlenecks that were present in LN control plants were relieved. Three of them were common with those relieved by *R. irregularis* (photosynthesis, purine and pyrimidine metabolism, aromatic acid metabolism), the fourth one is involved in ascorbate and aldarate metabolism. The HN treatment created 14 new metabolic bottlenecks compared to LN control conditions. These new bottlenecks are involved in glycolysis, TCA cycle, Calvin cycle, metabolism of Alanine, aspartate, glutamate, pyrimidine, purine, fructose, mannose, aromatic amino acids. These data indicate that different metabolic processes are modulated by N supply and *R. irregularis* inoculation. The most interesting result

is the fact that photosynthesis, pyrimidine metabolism, aromatic amino acid biosynthesis are 3 processes likely to play key roles on *R. irregularis* mediated N nutrition in maize.

**Transcriptome of *R. irregularis* in inoculated maize roots is driven by N availability**

To gain insight into the metabolic cross talk between *R. irregularis* and maize, we investigated the biological processes taking place in the fungal partner according to the N supply conditions. For this purpose, we determined the fungal genes displaying a higher expression in LN roots compared to HN roots and vice versa. This selection was performed for B73 and Lo3 separately. The Venn diagrams in Figure 9A and B show that under LN, 1251 fungal genes were up-regulated in Lo3 while they were 1247 in B73, including 548 transcripts up regulated in both maize lines. In HN roots, 1596 fungal transcripts were up-regulated in Lo3 and 1359 were up-regulated in B73 roots including 609 genes up-regulated in both maize lines. In both maize lines, the functional categories overrepresented in *R. irregularis* DEG were similar in each N nutrition condition Figure 9C. However, an important remodelling in *R. irregularis* overrepresented DEG functional categories in response to N supply was observed. For example, fungal genes up regulated under LN were involved in nuclear structures, vesicular trafficking, translation and transcription, whereas those up-regulated under HN had a role in metabolic activity of primary and secondary metabolism, in particular nucleotide and lipid metabolism. Only few maize line specific functional categories could be observed. For instance, defence mechanisms was a functional category of *R. irregularis* DEGs specifically expressed in Lo3. These data show that the fungal transcriptome is strongly affected by the nutritional N status of the host and the soil. Among the DEG functional categories, several genes were involved in amino acid and nucleotide metabolism and transport as well as in inorganic transport. We focused on the expression profiles of nucleotide and amino acid metabolism genes and transporter genes as well as phosphate and ammonium acid transport genes. Supplementary Table 7 shows the expression pattern of these fungal genes. Interestingly, fungal ammonia transporters are more highly expressed under LN than under HN. We did not find any fungal nitrate transporter genes in the differentially expressed AMF

genes. The fungal amino acid biosynthetic genes up regulated are mainly involved in asparagine, arginine, glutamine, glutamate and serine pathways. Several fungal amino-acid transporter genes were found up-regulated either in LN or HN roots. The fungal nucleotide biosynthesis genes up-regulated in HN roots are related to pyrimidine de novo biosynthesis or salvage pathways.

## Discussion

Due to the detrimental impact of chemical nitrogen (N) fertilizers used in maize production on the environment, it is urgent to find alternative agricultural practices to maintain yield and food quality while reducing their input (Yu *et al.*, 2022). Exploiting the beneficial effect of Arbuscular Mycorrhizal Fungi (AMF) on soil N capture by maize plants can be one of these practices (Dellagi *et al.*, 2020). Thus, to better understand the biological and genetic basis of such a beneficial effect, we have investigated the physiological and molecular responses of different maize genotypes when they are inoculated with the AMF *R. irregularis*. Plants were grown under three levels of N fertilization in order to identify key steps involved in the efficiency of the symbiotic association in terms of plant N uptake and N utilization.

In our study, the most interesting result was to find an increase in kernel yield in the two maize lines inoculated with *R. irregularis* when N nutrition is reduced. We showed that a symbiotic association with *R. irregularis* was able to compensate for maize plants performance when N fertilization is reduced. In the literature, depending on both the N supply level and the form of N supplied, different types of effects on yield and/or biomass production were reported, including an increase, no effect, or a reduction in productivity when the plant develops a symbiotic association with an AMF (Ingraffia *et al.*, 2020; Quiroga *et al.*, 2020; Yooyongwech *et al.*, 2022). In the present investigation, we estimated that kernel yield can be maintained with a 2- to 5-fold reduction in N input when two maize lines were selected based on the beneficial impact of an inoculation with *R. irregularis*. Such a beneficial impact was previously observed for maize plant biomass production under low N fertilizer inputs (Quiroga *et al.*, 2020). One can, therefore, conclude that the positive impact of AMF on plant performance can be variable depending on the AMF and the host plant species and genotypes as well as the level and type of available N source (Verzeaux *et al.*, 2017; Ingraffia *et al.*, 2020; Xie *et al.*, 2022)

Our transcriptome study allowed us to provide an overview of biological processes putatively involved during the establishment of a symbiotic association between the AMF *R.irregularis* and maize.

In the leaves of inoculated plants, four maize genes were found to be differentially expressed irrespective of the N-feeding conditions and the genotype (Zm00001d015569, Zm00001d043505, Zm00001d010039, Zm00001d006835). Zm00001d015569 was up-regulated and encodes a putative H+-proton pumping pyrophosphatase involved in vacuolar transport of inorganic ions. It has been shown that a wheat orthologue of this gene plays an important function in plant biomass production (Menadue *et al.*, 2021), suggesting that in inoculated plants, it could also be involved in the control of maize agronomic performances. Zm00001d043505, also up-regulated, encodes a putative histidine-kinase, which is putatively involved in cytokinin signaling (Yonekura-Sakakibara *et al.*, 2004), a process essential for maize growth (Sakakibara *et al.*, 2006; Cho *et al.*, 2022). The third gene, Zm00001d010039, was down-regulated and encodes a cellulose domain-containing protein, which could be involved in cell wall remodeling during leaf growth in symbiotic plants. The same pattern of expression was observed for Zm00001d006835, which encodes a putative transcription factor of the NF-Y family. This family of plant transcription factors is involved in the regulation of nitrate transporters, in the control of carbon/nitrogen, the regulation of flowering, and in drought tolerance in maize (Su *et al.*, 2018; Cheng *et al.*, 2021). Although these four genes did not allow us to identify a core biological process occurring in inoculated plants, their function was representative and biologically relevant of an interaction with an AMF.

Whatever the level of N fertilization or the two inoculated maize lines, the core DEGs that were either up or down-regulated in roots were enriched in transcripts encoding proteins involved in a variety of biological functions such as defense mechanisms, hormone signaling (especially jasmonate and cytokinin), N and C metabolism, cell wall and chromatin remodeling, proteolysis inhibition, metal homeostasis, phenylpropanoid and lipid metabolism. Similar results were previously obtained in several other model and crop species, indicating that most of these

biological functions are shared when the plant develops symbiotic associations with AMFs (Fiorilli *et al.*, 2009; Gallou *et al.*, 2012; Schaarschmidt *et al.*, 2013; Meng *et al.*, 2015; Handa *et al.*, 2015; Vangelisti *et al.*, 2018; Kaur and Suseela, 2020; Wang *et al.*, 2020; Hui *et al.*, 2022).

We also observed that a number of biological processes modified in the presence of the fungus were specific to each of the two maize lines. For instance, under LN in Lo3, autophagy-related genes were overrepresented among those that were upregulated. Nitrogen remobilization involving autophagy is known to provide N assimilates necessary for kernel filling (Li *et al.*, 2015). In B73, transcripts for genes involved in defense mechanisms were overrepresented when N fertilization was reduced. Although the role of plant immunity in the *Rhizobium*/legume $N_2$-fixing symbiotic association is well established, further work will be required for its characterization in AMF plant symbioses (Tóth and Stacey, 2015). In agreement with a study performed on Cassava inoculated with *R. irregularis* (Mateus *et al.*, 2019), our transcriptomic analysis indicates that there is a genotypic variability of the molecular response in terms of gene transcription, and that this genotypic variability is dependent upon N nutrition.

The fact that several biological processes enriched in the functional GO categories corresponded to the cognate metabolic pathways is worth highlighting. For instance, changes in the level of expression of genes involved in sugar, amino acid, and lipid metabolism were confirmed by metabolomics analyses (Supplementary Figure 8 and 9). Under HN, the amounts of root soluble carbohydrates sucrose, fructose, and glucose were lower in inoculated plants compared to controls, which is consistent with the export of C-containing molecules to the fungus. As this did not occur under LN, one can hypothesize that the roots and/or the fungus do not constitute an important sink for C or that the plant is able to limit fungal proliferation under N-limiting conditions. Under LN, genes involved in the control of plant immunity were up-regulated in roots of inoculated plants, especially in line B73, which is consistent with the accumulation of shikimic acid (Supplementary Figure 8). It is possible that the process controlling plant immunity limits proliferation of the fungus and thus its C sink capacity. Both

transcriptomic data and metabolomics data show modifications in lipid metabolism and the accumulation of lipids in roots. In roots, when N fertilization was not limiting, we observed an accumulation of two lipids, trans-13-octadecenoic acid and palmitoleic acid (Supplementary Figure 8). Lipid accumulation in roots colonized by AMFs was already observed (Keymer *et al.*, 2017; MacLean *et al.*, 2017), notably in *R. irregularis*, to which their reduction and transfer from the host to the fungus is considered to be a way of fueling the symbiotic fungus with a carbon source other than sugars (Keymer *et al.*, 2017; MacLean *et al.*, 2017). In the present study, lipid accumulation occurred only under HN, which is consistent with the fact that due to higher photosynthetic activity revealed by the accumulation of soluble carbohydrates, the plant is able to synthesize more fatty acids to feed the fungus.

Interestingly, we found that in inoculated plants, Arginine (Arg), known to be a key molecule involved in the transfer of N from the fungus to the plant (Chen *et al.*, 2018*a*; Kaur and Suseela, 2020; Dellagi *et al.*, 2020), accumulates under HN conditions not only in the roots of line B73 HN but also in the leaves (Bago *et al.*, 2001; Dellagi *et al.*, 2020; Xie *et al.*, 2022). Another process that appears to be playing a crucial role in AMF symbiosis is the downregulation of pyrimidine biosynthesis in inoculated plants, which indicates that pyrimidine biosynthesis can be an essential process for plant N management (see below) (Zrenner *et al.*, 2006; Fernie *et al.*, 2020). In alignment with this observation, our research reveals that nucleotide metabolism, particularly the accumulation of pyrimidines, plays a pivotal role in both plant nitrogen (N) nutrition and, consequently, plant biomass production in the context of the symbiotic association with arbuscular mycorrhizal fungi (AMF). Our transcriptomic analysis demonstrates that, regardless of nitrogen feeding conditions, pyrimidine biosynthesis processes are consistently downregulated in leaves of inoculated plants (Figure 5).

Furthermore, under low nitrogen (LN) conditions, several genes encoding enzymes involved in nucleotide metabolism, including carbamoyl-phosphate synthase (Witte and Herde, 2020*b*), are downregulated in both leaves and roots of maize lines Lo3 and B73 (Figure 5, Supplementary Table 8). Notably, these genes are also downregulated in B73 roots when

inoculated with *R. irregularis* under LN conditions (Supplementary Table 8). A critical enzyme in this context is Zm00001d023833, encoding a putative nucleoside diphosphate kinase (NDPK), which participates in UTP and TTP biosynthesis through nucleotide salvage (Witte and Herde, 2020*a*). Our data indicate that under nitrogen deficiency, nucleotide metabolism undergoes alterations that may negatively impact plant yield. In the symbiotic association, NDPK gene expression remains unaltered, suggesting the absence of constraints on this enzymatic reaction (Supplementary Table 8). This implies that AMF likely supplies the host plant with nucleotides and nucleosides, potentially pyrimidines, to circumvent the deficiency in NDPK activity, thereby alleviating the associated metabolic bottleneck. This observation is consistent with the known role of NDPK in plant survival with respect to pyrimidine salvage (Tegeder, 2014; Witte and Herde, 2020*a*).

Pyrimidine metabolism holds significance not only in crop performance but also in nitrogen use efficiency (NUE) (Tegeder, 2014; Lee *et al.*, 2018; Melino *et al.*, 2022). Recent findings demonstrate a correlation between maize leaf nitrogen accumulation and NDPK protein levels (Urrutia *et al.*, 2023), further supporting the hypothesis that *R. irregularis* stimulates the reprogramming of plant pyrimidine metabolism to enhance maize performance under nitrogen-limiting conditions. Allantoin and allantoic acid, metabolites associated with pyrimidine, likely play a crucial role in the nitrogen economy of the symbiotic interaction. Allantoin can be converted to allantoic acid via allantoinase. We observed higher allantoin levels in the roots of plants grown under high nitrogen (HN) conditions compared to LN. Additionally, a gene encoding allantoinase was upregulated following *R. irregularis* inoculation in maize roots under both LN and HN conditions (Supplementary Table 8). Simultaneously, the fungus upregulates a gene encoding allantoicase, an enzyme that converts allantoic acid to urea, suggesting the fungus releases the latter. However, we did not detect variations in allantoin levels in inoculated plant roots compared to non-inoculated plants and did not detect allantoic acid (Supplementary Figure 8). Further investigations are required to elucidate the role of ureides in the nitrogen economy of the symbiotic association, as limited reports suggest mycorrhizal fungi's potential

to produce ureides or induce allantoin and allantoic acid production in plants (BARROSO *et al.*, 1988; Thakur and Garg, 2023).

The integration of maize and fungal RNAseq and metabolome analyses has allowed us to construct a simplified model depicting the various biological events occurring in the symbiotic association (Figure 10). As fungal arbuscules are known to undergo controlled senescence (Choi *et al.*, 2018; Paries and Gutjahr, 2023), our data suggest that autophagy is upregulated in both maize genotypes under both HN and LN conditions, with higher expression in Lo3 LN roots. Autophagy likely contributes to the degradation of fungal cellular products, potentially releasing nucleosides. The nucleotide salvage process can then recycle nucleosides. Nucleosides and pyrimidines produced by inoculated tissues may repress de novo plant pyrimidine biosynthesis pathways (Tegeder, 2014; Witte and Herde, 2020*b*).

Under LN conditions, limited nitrate ($NO_3^-$) is available to both the fungus and the plant. In living fungal cells, RNAseq data indicate the upregulation of amino acid transporters and ammonium transporters, some of which may be located at the extraradical mycelium (ECM), at the intraradical mycelium (IRM) and at the peri-arbuscular membrane (PAM) interfaces. Fungal argininosuccinate synthase and arginase genes are upregulated under LN, potentially leading to urea accumulation. A fungal urea transporter is also upregulated under LN. Urea is likely further degraded into ammonium by urease, as the fungal urease-coding gene is upregulated under LN. This could explain the observed lower urea levels in *R. irregularis* inoculated roots under LN (Supplementary Figure 10). Additionally, lower levels of amino acids are found in LN roots, suggesting reduced assimilation via the glutamine synthetase-glutamate synthase (GS-GOGAT) pathway in fungal and inoculated plant root cells. Fungal RNAseq data indicate the downregulation of pyrimidine de novo biosynthetic genes and the pyrimidine salvage pathway under LN, implying that the fungus redirects its nitrogen metabolism to provide ammonium to the plant cell. Under HN conditions, where ample $NO_3^-$ is available, fungal RNAseq data indicate the upregulation of specific amino acid transporters distinct from those in LN conditions, along with the downregulation of ammonium permeases. Fungal argininosuccinate

synthase and arginase genes are downregulated under HN, potentially leading to urea accumulation. A fungal urea transporter is downregulated under HN. Urea is likely converted into ammonium by an unidentified urease. Increased levels of various amino acids, including citrulline, a precursor of arginine, are observed in HN-inoculated roots. Arginine and asparagine accumulate in these roots, suggesting upregulation of fungal and/or plant assimilation via GS-GOGAT under HN conditions (Supplementary Figure 10). Pyrimidine de novo biosynthetic genes and the pyrimidine salvage pathway are upregulated in HN roots. Allantoin accumulates exclusively in HN roots and remains unaffected by inoculation. This metabolite can be converted into allantoic acid, which may be released into the apoplast (Tegeder, 2014). A fungal allantoicase is upregulated in HN roots, indicating possible conversion of allantoic acid into urea under HN conditions. This transfer of ureides is akin to the process observed in symbiotic associations between tropical legumes and Rhizobia species (Tegeder, 2014). Previous studies have also identified upregulation of genes involved in allantoin synthesis in roots of AMF-inoculated plants (Nanjareddy *et al.*, 2017). Consequently, it is plausible that ureide transfer mirrors that occurring in legume nodules. These findings suggest that under HN conditions, the fungus adjusts its nitrogen metabolism to provide pyrimidines to the plant cell. Collectively, these data reveal a molecular cross-talk between plant and fungal pyrimidine pathways. The dataset used to construct this model are presented in Table 1, Supplementary Table 7 and 8; and Supplementary Figure 10.

In conclusion, we propose that inoculating maize with *R. irregularis* offers a promising strategy to significantly reduce nitrogen fertilizer usage while maintaining maize kernel yield. Our findings highlight a metabolic interplay between the host and AMF, with pyrimidine and ureide metabolism serving as key players in this interaction. Furthermore, the observed differences in how our two studied maize lines embrace different strategies to benefit from the fungus illustrate the importance of leveraging maize's extensive genetic diversity for a comprehensive understanding of this symbiotic interaction (Schmidt *et al.*, 2016; Sawers *et al.*, 2018*b*; Liu *et al.*, 2020).

919

## Data Availability

RNAseq project is deposited (Gene Expression Omnibus,Edgard R. et al. 2002): https://www.ncbi.nlm.nih.gov/geo/query/acc.cgi?acc=GSE235654 ; accession no. GSE235654. All steps of the experiment, from growth conditions to bioinformatic analyses, were detailed in CATdb (Gagnot *et al.*, 2008): http://tools.ips2.u-psud.fr.fr/CATdb/; Project: NGS2021_19_Rhizophagus according to the MINSEQE 'minimum information about a high throughput sequencing experiment'.


## Acknowledgments:

BD acknowledges Université Paris Saclay for PhD fellowship. AD acknowledges the benefits received from France 2030 program (Saclay Plant Sciences, reference n° ANR-17-EUR-0007, EUR SPS-GSR integrated into France 2030 (reference n° ANR-11-IDEX-0003-02), INRAE Grant IB BAP 2021 MYCORN, and IJPB's Plant Observatory technological platforms. RS gratefully acknowledges funding support from National Science Foundation (NSF) CAREER grant (1943310) and Nebraska Collaboration Initiative Grant (21-1106-6011). We thank Michel Lebrusq, Lilan Diahuron, Patrick Grillot, and Christian Jeudy for taking care of the plants in the greenhouse. We thank the POPS platform for the RNAseq experiment and data. We also thank Etienne Delannoy from POPS platform for fruitful discussions. We are grateful to Cyril Bauland and Carine Palaffre from the INRAE for providing seeds from the Centre de Ressources Biologiques of Saint Martin de Hinx (France). We acknowledge Pr. Mario MOTTO from ISC, Bergamo (Italy) for providing Lo3 seeds.

**Table 1** : **List of metabolic bottlenecks relieved and created by *R. irregularis* or N supply.** Metabolic bottlenecks were identified by MBA that are relieved by either R. irregularis treatment or HN treatment compared to LN control conditions are indicated as “debottlnecked”. Those that were newly created following R. irregularis or HN treatment were compared to LN control conditions are indicated as “new metabolic” bottelnecks.

| **Reactions Debottelnecked by *R. irregularis* treatment** | |
|---|---|
| **R03817[M,t]** | Photosynthesis light reactions |
| **R00124[R,p]** | Purine and Pyrimidine metabolism |
| **R00692[R,p]** | Phenylalanine, tyrosine, and tryptophan metabolism |
| **R04241_mod[R,m]** | Folate metabolism |
| **Reactions Debottelnecked by HN treatment** | |
| **R03817[M,t]** | Photosynthesis light reactions |
| **R00124[R,p]** | Purine Pyrimidine metabolism |
| **R00692[R,p]** | Phenylalanine, tyrosine, and tryptophan metabolism |
| **R00095[R,x]** | Ascorbate and aldarate metabolism |
| **New metabolic bottlnecks with LN RHIZO** | |
| **R03346[M,c]** | Nicotinate and nicotinamide metabolism |
| **R03346[B,c]** | Nicotinate and nicotinamide metabolism |
| **R00086[M,pm]** | Purine metabolism |
| **R00986[R,p]** | Purine metabolism |
| **MR00968[B,c]** | Benzoate metabolism |
| **R00086[B,pm]** | Purine metabolism |
| **R00341[R,c]** | Pyruvate metabolism |
| **R00216[B,p]** | Pyruvate metabolism |
| **R01058[B,c]** | Glycolysis |
| **R02678[R,m]** | Phenylalanine, tyrosine, and tryptophan metabolism |
| **R00710[R,m]** | Pyruvate metabolism |
| **R01067[R,c]** | Calvin-Benson-Bassham cycle |
| **R01067[R,p]** | Calvin-Benson-Bassham cycle |
| **New bottlnecks in HN** | |
| **R00341[R,c]** | Pyruvate metabolism |
| **R00709_mod[R,m]** | TCA cycle |
| **R00713[R,m]** | Alanine, aspartate, and glutamate metabolism |
| **R01067[R,c]** | Calvin-Benson-Bassham cycle |
| **R01067[R,p]** | Calvin-Benson-Bassham cycle |
| **R01667[R,p]** | Pyrimidine metabolism |
| **R00235[B,x]** | Pyruvate metabolism |
| **R00885[B,c]** | Fructose and mannose metabolism |
| **R01058[B,c]** | Glycolysis |
| **R02080[M,c]** | Phenylalanine, tyrosine, and tryptophan metabolism |
| **R00214[M,m]** | Pyruvate metabolism |
| **R00124[B,p]** | Purine metabolism |
| **R00267_mod[M,c]** | Alanine, aspartate, and glutamate metabolism |

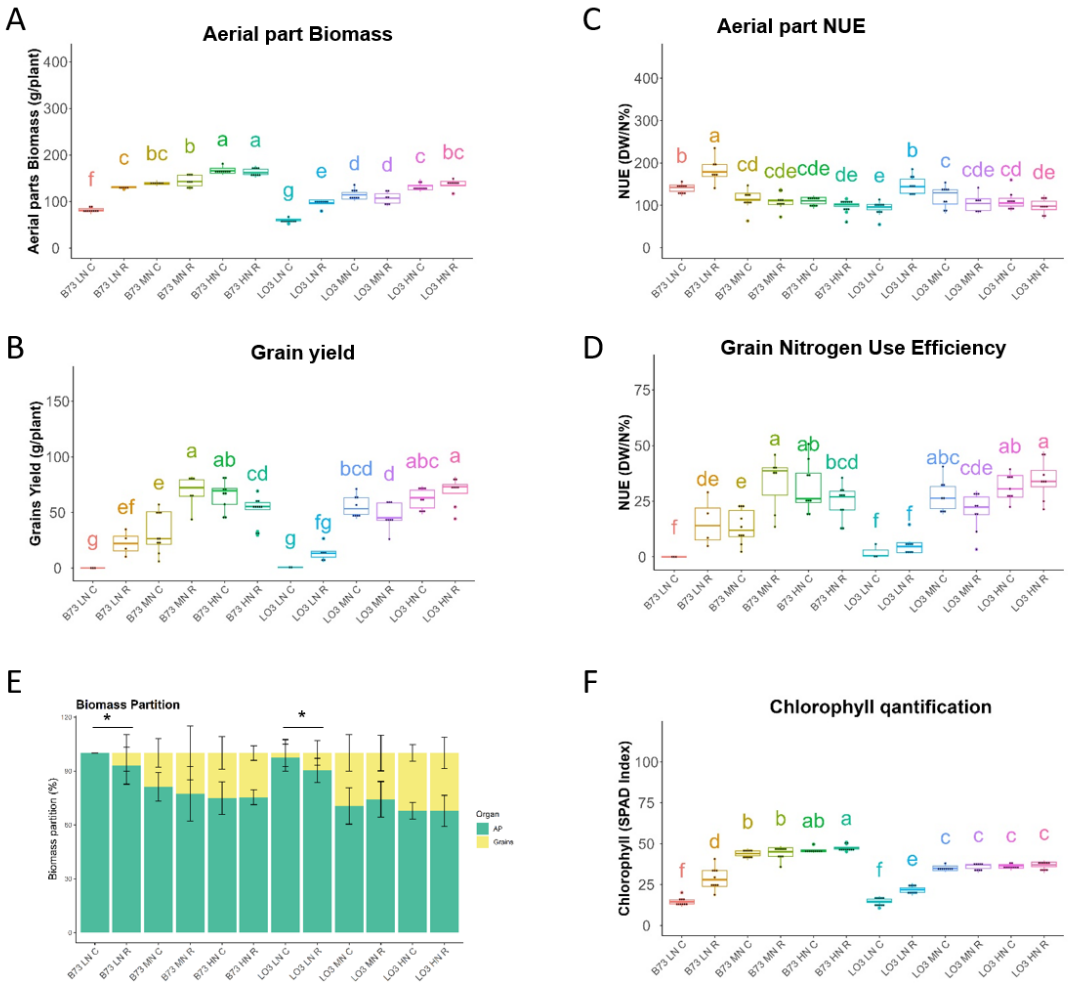


**Figure 1: Impact of N supply on maize responsiveness to *R. irregularis* for biomass and N content shows that beneficial effects are more pronounced at LN. A** and, **B** : Biomass of grains and aerial parts of indicated samples. **C,D** : Nitrogen Use Efficiency (NUE) in grains and vegetative aerial parts of indicated samples. **E**: Biomass partitioning F: Average chlorophyll content measured on leaves 4,5 and 6 over 5 weeks after sowing. C: control, R: *R. irregularis,* AP: Biomass of Aerial Parts. N=7 to 10 plants for grains and AP, and N=5 for roots. Different letters indicate significantly different averages for the considered trait by ANOVA, a star indicates significant difference between control and inoculated plants,

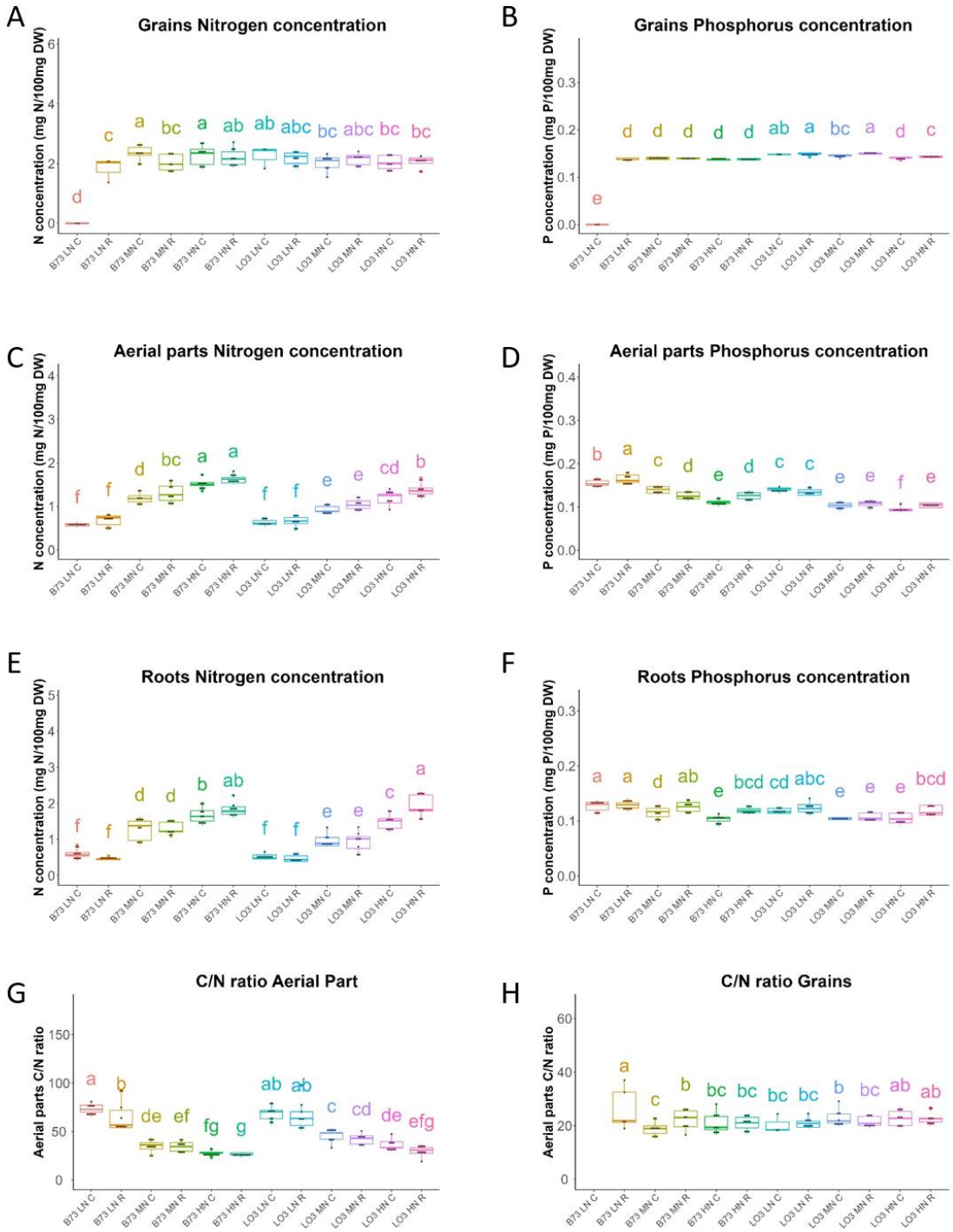


**Figure 2: Impact of N supply on maize responsiveness to *R. irregularis* for P and N content and C/N ratio highlights poor impact of AM symbiosis on these traits. A** to **F** : N and P content of grains, aerial parts and roots. **G** and **H** C/N ratios in aerial parts and grains. C: control, R: *R. irregularis* N=7-10 plants for grains and aerial parts. N=5 for roots. Different letters indicate significantly different averages for the considered trait by ANOVA.

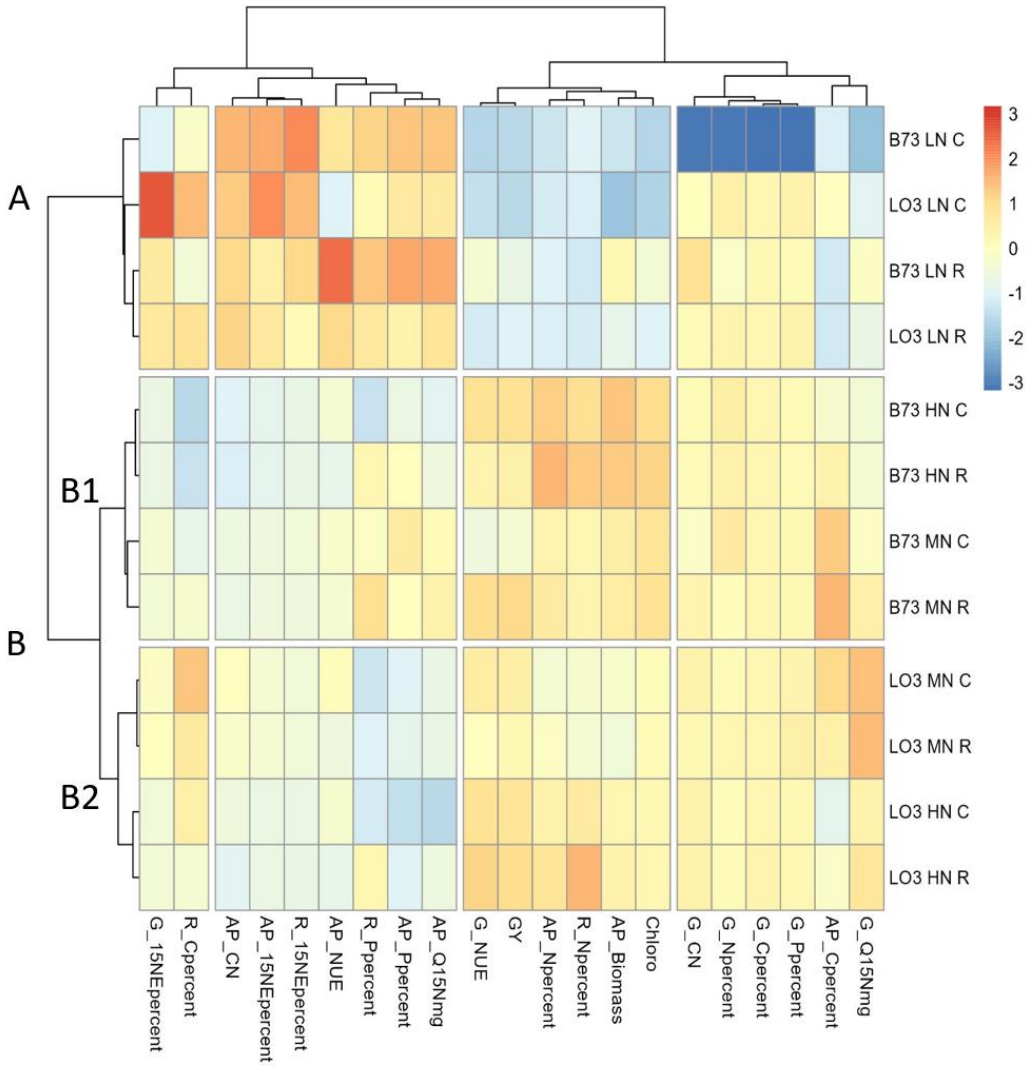


**Figure 3: Heatmap representing of physio-agronomical traits in different organs shows that *R. irregularis* of LN plants improves their performances.** Heat map showing the standardized level of physio-agronomic traits of B73 and LO3 lines under LN, MN or HN inoculated or not with *R. irregularis*. The two HCA were performed to group the samples and the physio-agronomic traits according to their average values following Ward method of clutering. At the left of the HCA, the vertical bar represents the groups of samples. Indicated traits are measured in Aerial parts (AP), roots (R) or grains (G). Group A corresponds to plants grown under LN, Group B corresponds to plants grown under MN or HN. The B group is subdivided into two subgroups: B1 and B2 correspond respectively to B73 and LO3 plants. AP: Aerial Parts, G: grains, R: Roots. Cpercent: Percentage of C. Npercent: percentage of N. 15NEpercent: percentage of 15N. P Percent: percentage of P. NUE: Nitrogen Use Efficiency. GY: Grain Yield. Details for calculate these traits are indicated in Supplementary Table 3.

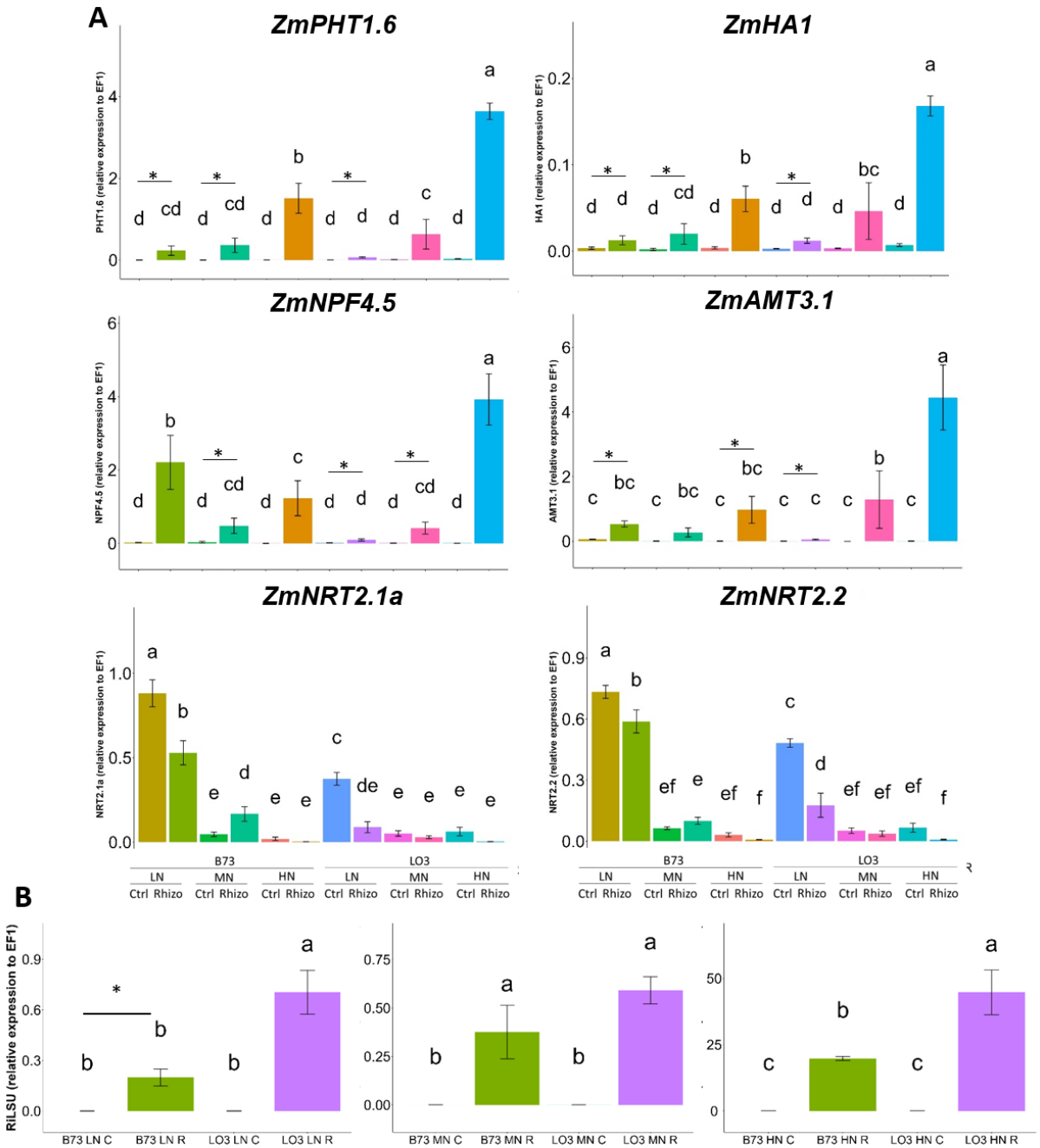


**Figure 4: Impact of N supply on expression of genes involved in N and P transport in roots suggest that AM symbiosis alleviates N deficiency stress.** Plants were grown under LN, MN or HN and inoculated or not with *R. irregularis*. Roots were harvested at VT+15 stage. **A**: Normalized transcript levels of indicated genes monitored by qRT-PCR. **B:** Quantification of *R. irregularis* in roots by qRT-PCR amplification of the *RiLSU* constitutive fungal transcript. C: control, R: *R. irregularis;* N=5. Different letters indicate significantly different gene expression levels as analyzed by ANOVA. Bars are standard errors. Stars indicates significant difference between control and *R. irregularis* inoculated plants by t-test.

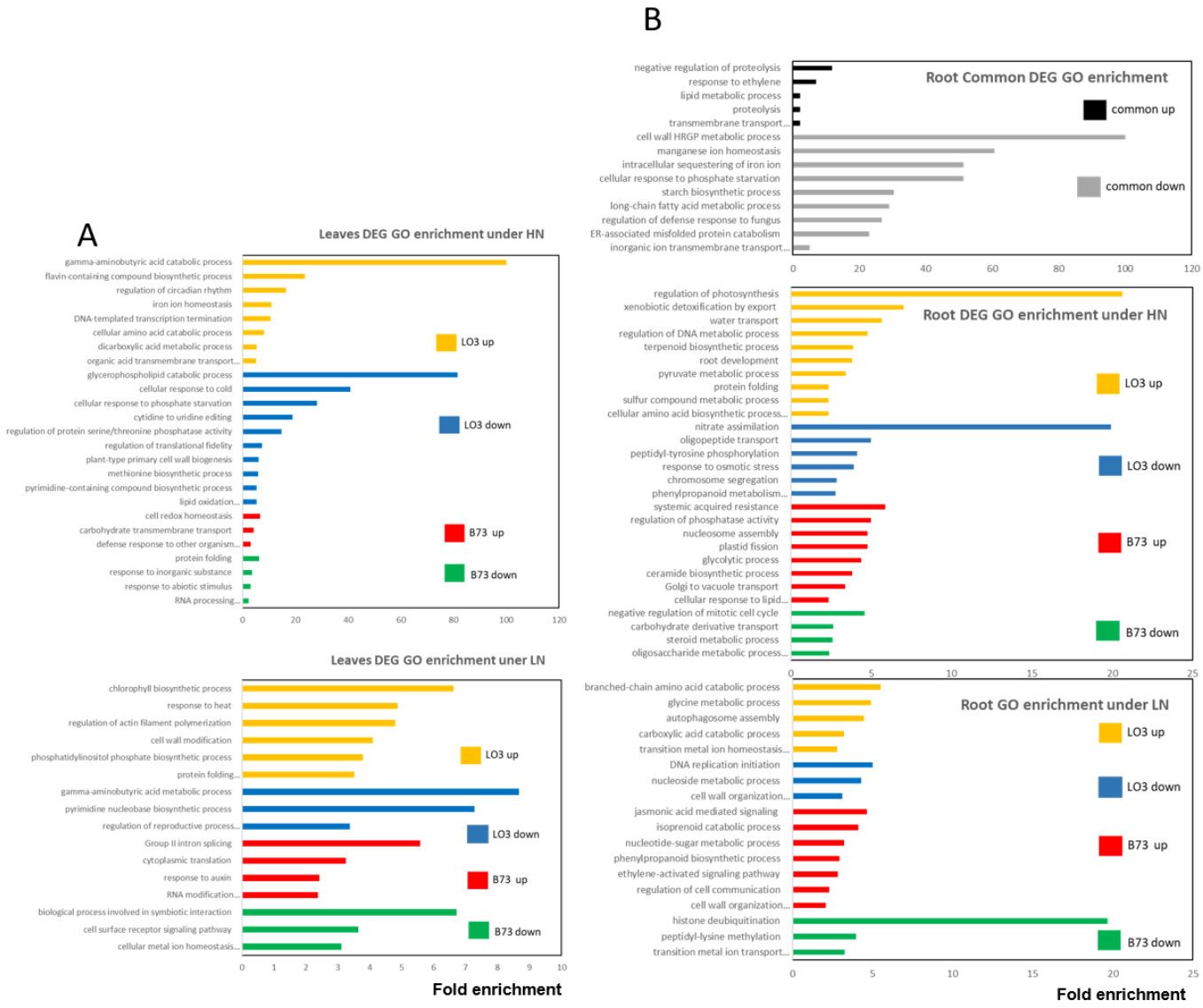


**Figure 5 : Gene ontology of the enriched functional categories in the common DEG. A:** Leaf genes and **B**: Root genes. Common DEGs were selected so that they have the same pattern of regulation (up or down) in the different conditions with a FC >1.5. FC represents the ration of expression of each gene in *R. Irregularis* inoculated tissues versus the control. There were only 2 genes in the common DEGs in leaves thus, they were not included in the GO analyses. Each bar represents the fold enrichment in the indicated category obtained by https://pantherdb.org/. Only categories enriched more than 2 fold and displaying more than 2 genes are represented with *p*-value of enrichment < *0.05* are represented .

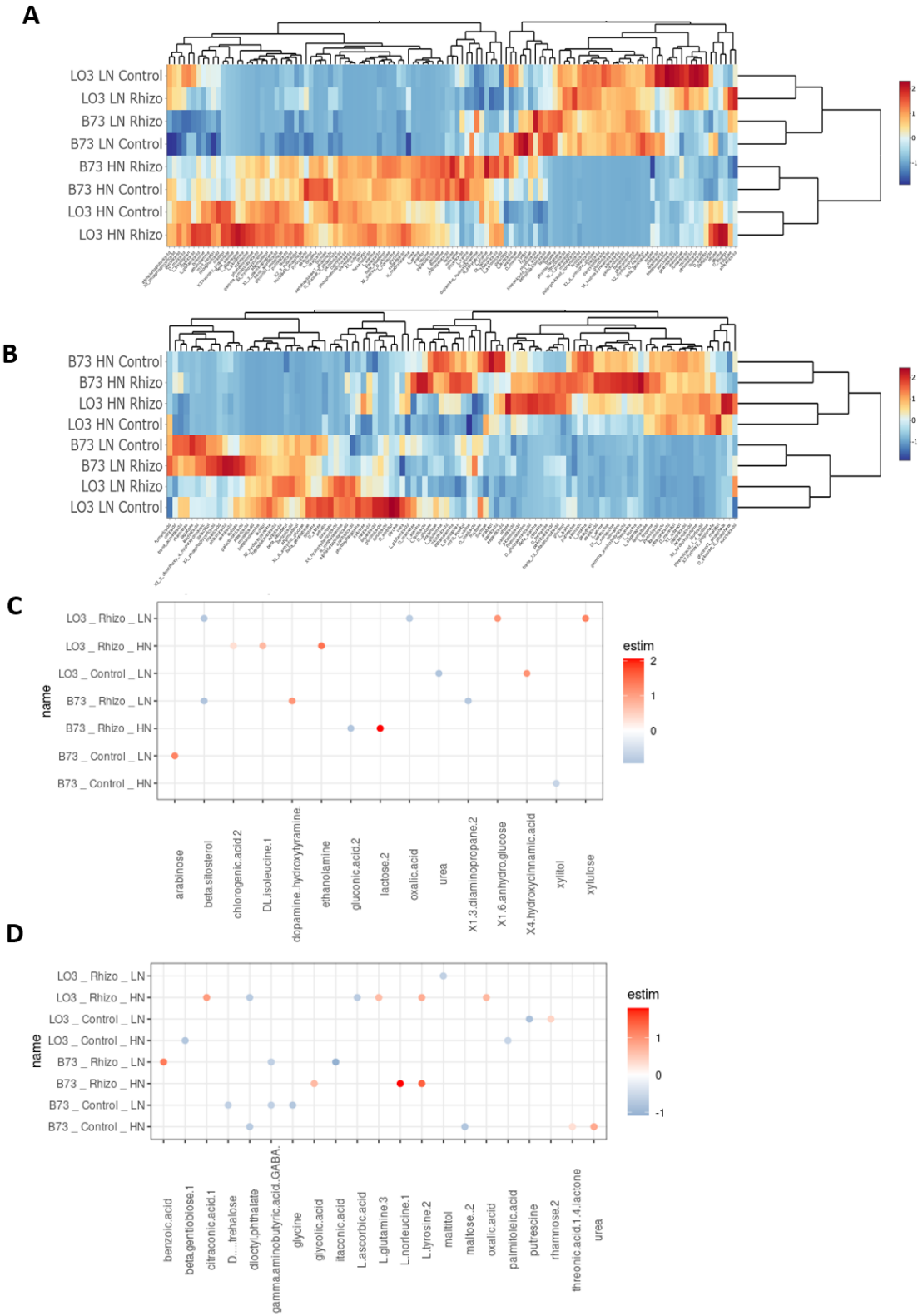


**Figure 6: Metabolomic analyses of leaves and roots at VT+15 stage reveals key metabolites specific to symbiosis under LN or HN nutrition. A** and **B :** HCA heatmap showing metabolomic profiling of leaves and roots of inoculated or control plants under LN or HN in leaves and roots respectively. **C** and **D**: Analyses of metabolomics data conducted with the R package MultiVarSel with a threshold of 0.884 showing the metabolites on which the genotype, the N nutrition of the R. irregularis inoculation have an impact. The color scale indicates if the metabolites are accumulated (red) or down accumulated (blue) in the indicated conditions with respect to the others.

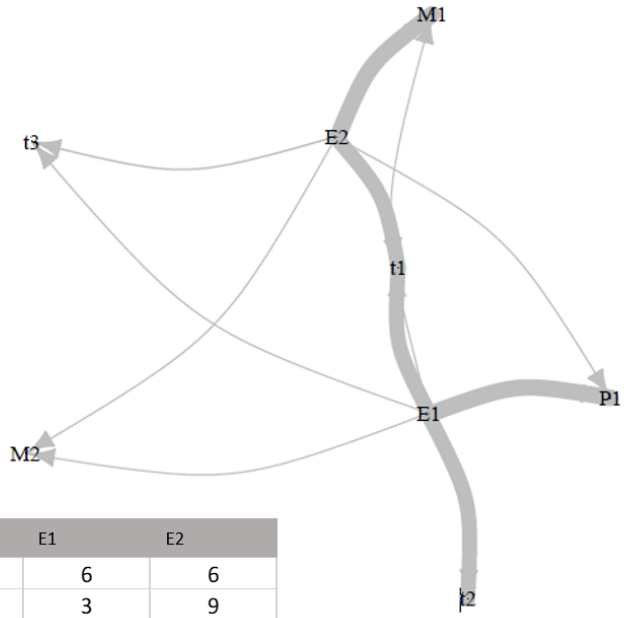


| Experiment Conditions | E1 | E2 |
|---|---|---|
| CTRL | 6 | 6 |
| RHIZO | 3 | 9 |
| B73 | 4 | 8 |
| LO3 | 6 | 7 |
| HN | 6 | 6 |
| LN | 3 | 9 |

**Figure 7 : Integrated clustering of metabolomics, transcriptomics and physiological traits in roots.** The integration analysis found that the correlated clusters of samples are subdivided in two experiments (E1 and E2), three transcriptomics clusters (t1, t2 and t3), two metabolomics clusters (M1 and M2) and one cluster of physiological traits (P1) (Supplementary Table 6).

A

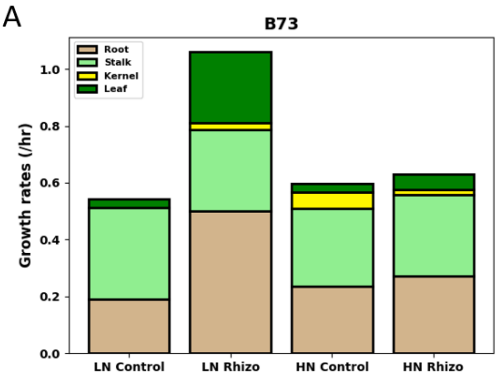


B

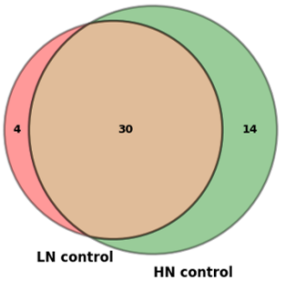


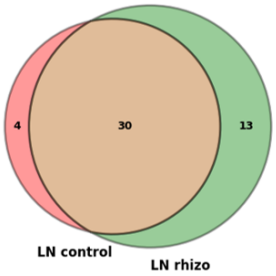


| Reactions Debottelnecked by HN treatment | |
|---|---|
| R03817[M,t] | Photosynthesis light reactions |
| R00124[R,p] | Pyrimidine metabolism |
| R00692[R,p] | Phenylalanine, tyrosine, and tryptophan metabolism |
| R00095[R,x] | Ascorbate and aldarate metabolism |

| Reactions Debottelnecked by *R. irregularis* treatment | |
|---|---|
| R03817[M,t] | Photosynthesis light reactions |
| R00124[R,p] | Pyrimidine metabolism |
| R00692[R,p] | Phenylalanine, tyrosine, and tryptophan metabolism |
| R04241_mod[R,m] | Folate metabolism |

C

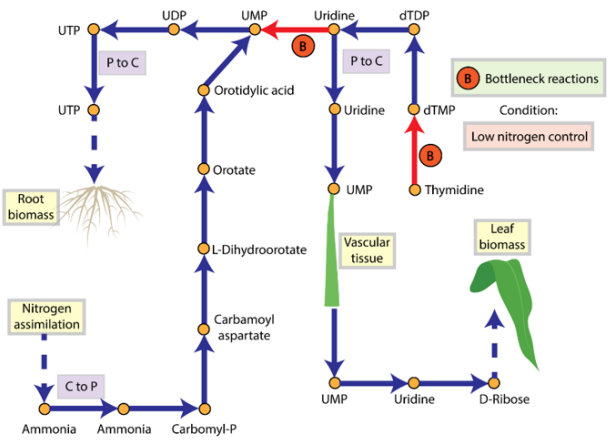


**Figure 8: Genome based metabolic modeling reveals essential impact of AMF on pyrimidine metabolism**. **A**: EXTREAM algorithm predicted higher yield under LN in B73. **B**: Venn diagrams showing the metabolic bottlenecks under indicated conditions highlighting the debottlenecked reactions. **C**: Metabolic reactions in the pyrimidine pathway common to the debottlenecked reactions by B73_LN_Rhizo, B73_HN compared to the corresponding B73_LN_Control.

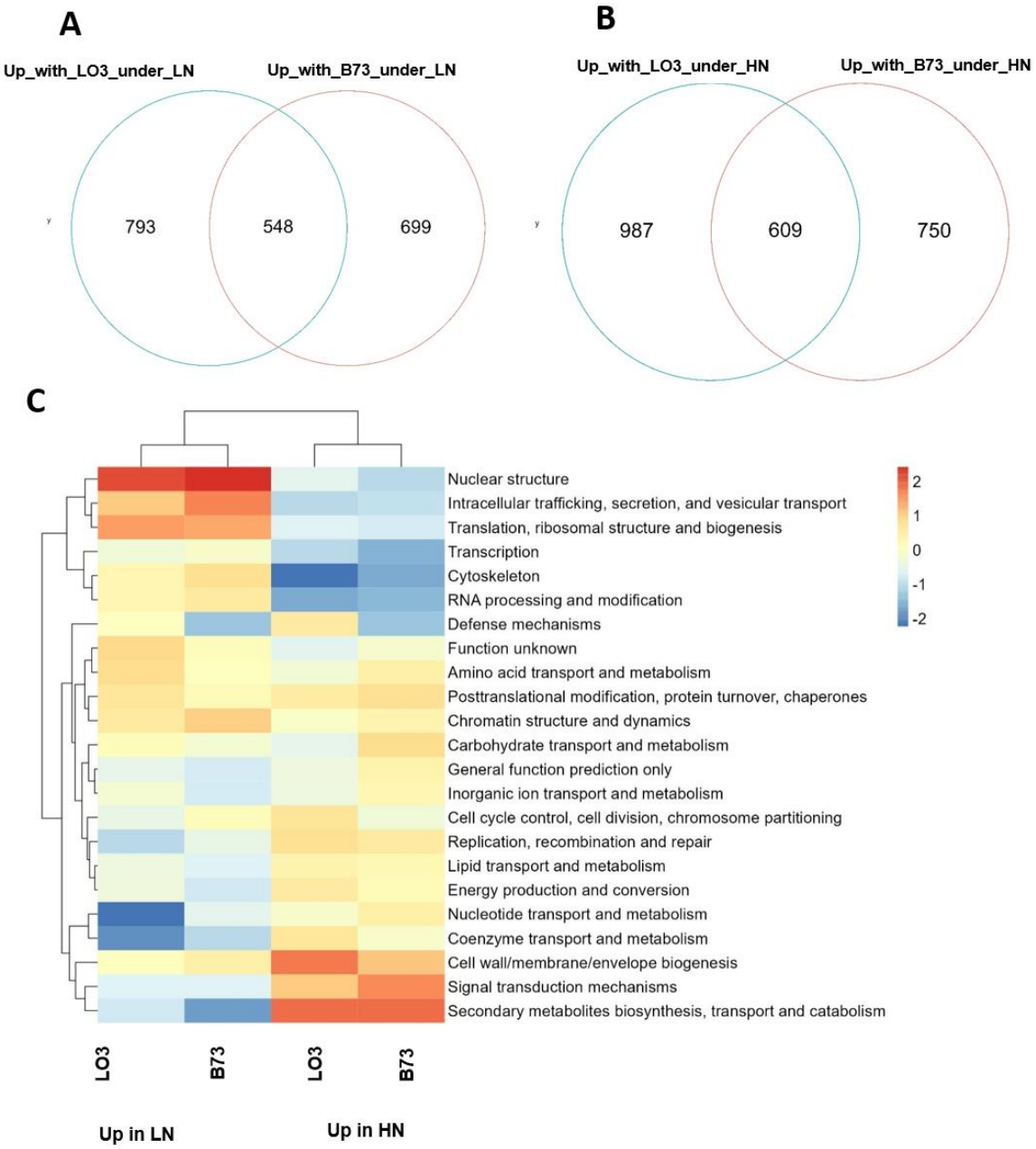


**Figure 9 : *Rhizophagus irregularis* transcriptome in maize roots is shaped by N supply.** Plants were grown under LN or HN. DEGs were selected so that they have FC >1.5. **A** : Up in LN indicates *R. irregularis* genes that are more highly expressed in LN compared to HN. **B**: Up in HN indicates *R. irregularis* genes that are more highly expressed in HN compared to LN. In **B**: Up_with_LO3_under_LN and Up_with_LO3_under_LN indicate fungal genes up-regulated under LN compared to HN in LO3 or B73 respectively. Up_with_LO3_under_HN and Up_with_LO3_under_HN indicate fungal genes up-regulated under LN compared to HN in LO3 or B73 respectively. **C**: Gene ontology of functional categories enrichment was based on KOG annotations of encoded proteins (see materials and methods). Each bar represents the functional category enriched in the given condition. p-value of enrichment was < 0.05; only categories enriched more than 2 fold and displaying more than 2 genes are represented and used to build the heatmap.

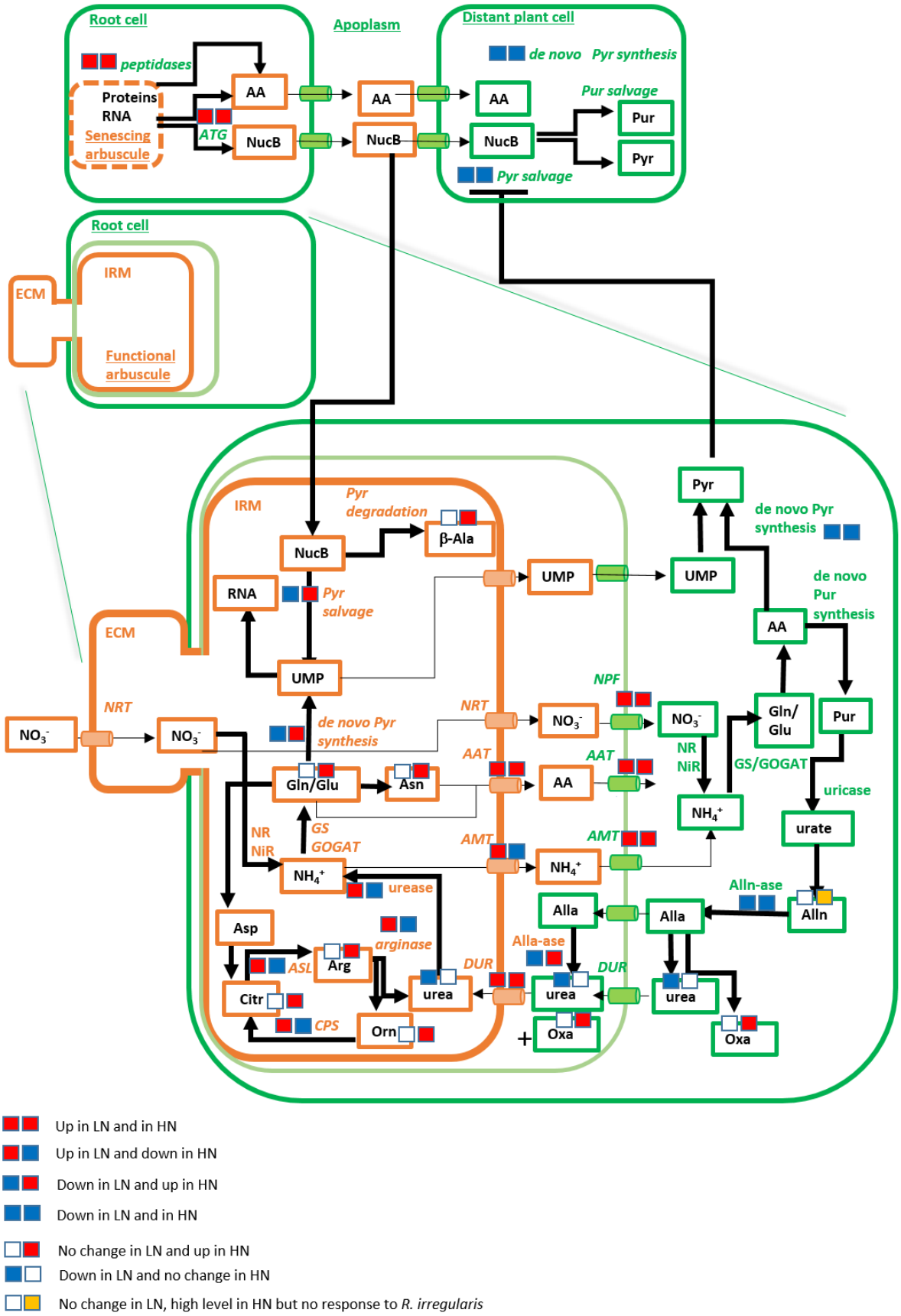


**Figure 10: Hypothetical working model for maize and *R. irregularis* N nutrition under LN and HN.** To build the model data from B73 and Lo3 maize lines were pooled for simplification (Supplementary

Figure 10, Supplementary Tables 7 and 8). Under LN **f**ungal RNAseq data indicate up regulation of amino acid transporters and ammonium transporters. Fungal argininosuccinate synthase and arginase genes are up regulated under LN, which could lead to urea accumulation. A fungal urea transporter is upregulated under LN. However, urea is probably further degraded into ammonium by urease since the fungal urease coding gene is up regulated under LN. This could explain the fact that under LN, *R. irregularis* inoculated roots accumulate less urea. Globally lower amounts of amino acids are found in LN roots which suggests less assimilation via GS-GOGAT in the fungal and inoculated plant root cells. The fungal RNAseq data indicate that pyrimidine de novo biosynthetic genes are down regulated under LN (for example, UMP synthase, orototate phosphorybolsyl transferase) as well as the pyrimidine salvage pathway (for example, dUTPase, allantoicase, deoxycitydylate deaminase, cytosine deaminase). These data suggest that under LN the fungus redirects its N metabolism in order to provide $NH_4^+$ to the plant cell. Under HN, high amounts of $NO_3^-$ are available to the fungus and to the plant. Fungal RNAseq data indicate up-regulation of some amino acid transporters that are different from those up-regulated in LN, down regulation of ammonium permeases. Fungal argininosuccinate synthase and arginase genes are down-regulated under HN, which could lead to urea accumulation. A fungal urea transporter is down-regulated under HN. Urea is probably further degraded into ammonium by another urease that we could not identify. We observe a global increase in the amounts several amino acids including Citr, which is a precursor of Arg. Arg and Asn accumulate in inoculated roots indicating that fungal and/or and plant assimilation via GS-GOGAT are probably upregulated under HN in response to the fungus. The fungal RNAseq data indicate that in HN roots, pyrimidine de novo biosynthetic genes are up-regulated (for example, UMP synthase, orototate phosphorybolsyl transferase) as well as the pyrimidine salvage pathway (for example, dUTPase, allantoicase, deoxycitydylate deaminase, cytosine deaminase). Allantoin accumulates only in HN roots and not in LN roots, and its amount is not affected by inoculation in HN roots. Allantoin can be converted into allantoic acid which can be released in the apoplast. In HN roots a fungal allantoicase is up-regulated indicating that urea is produced under HN. In italics, genes. In boxes: metabolites In orange : fungal genes or metabolites. In green : plant genes or metabolites. In front of genes and metabolites there are two squares. The square at the left indicates the status of the item under LN. The square at the right indicates the status of the item under HN. AA: Amino acids. NucB: Nucleobases. Pur: Purine. Pyr: Pyrimidine. IRM: Intraradical mycelium. ECM: Extraradical mycelium. .Alla: Allantoic Acid. Alln : Allantoin. Alln-ase: Allantoinase. Arg: arginine. Asn: Asparagine. Asp : Aspartate. b-Ala :b-alanine. Citr : Citrulline. Glu: Glutamate. Gln: Glutamine. Orn : Ornithine. GOGAT: Glutamine Oxo-Glutarate Aminotransferase. Oxa : Oxalic Acid. NR : Nitrate reductase. NiR : Nitrite reductase. AAT : Amino acid transporter. AMT : Ammonium transporter. DUR : Urea transporter. NPF : plant Nitrate transporter. NRT : R. irregularis nitrate transporter. CPS : Carbamoyl-phosphate synthase. ASL : Argininosuccinate lyase.

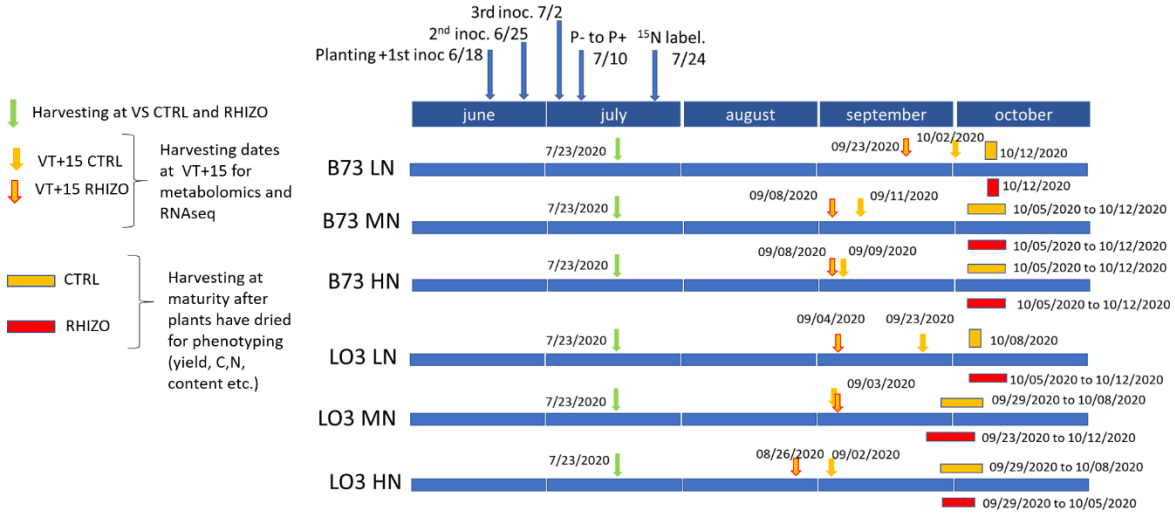


**Supplementary Figure 1: Experimental design with details for dates of each treatment and harvesting dates.** Experiments were performed at indicated dates on summer 2020 in the greenhouse. The top blue boxes indicate the months. Each month is represented on the boxes below for each maize line/condition. For each maize line/condition, the harvesting dates for the vegetative stage (VS) and 15 days after vessel tasseling (VT+15) stage are indicated. The horizontal red and yellow boxes indicate the periodes of harvesting dry mature plants for physio-agronomical traits phenotyping.

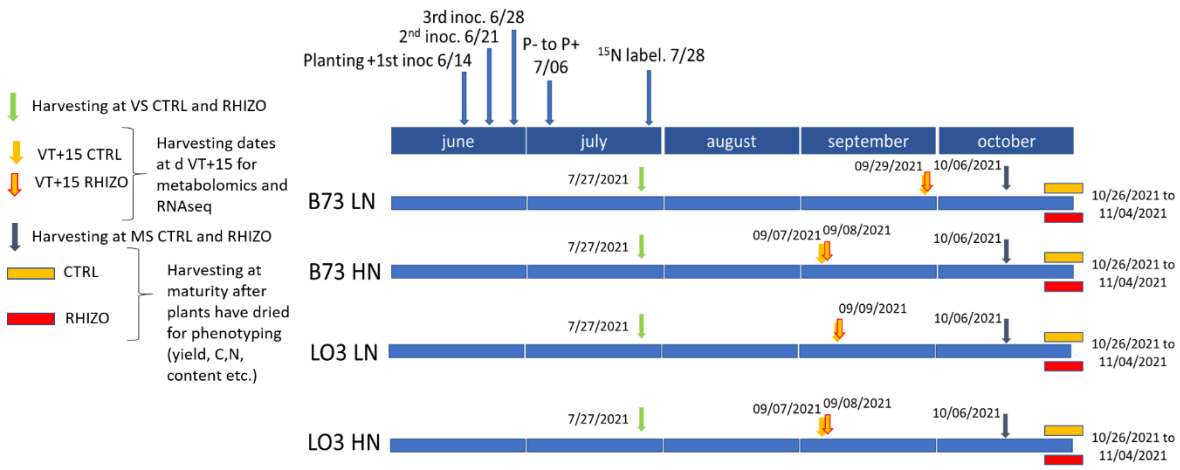


**Supplementary Figure 2: Experimental design with details for dates of each treatment and harvesting dates.** Experiments were performed at indicated dates on summer 2021 in the greenhouse. The top blue boxes indicate the months. Each month is represented on the boxes below for each maize line/condition. For each maize line/condition, the harvesting dates for the vegetative stage (VS) and 15 days after vessel tasseling (VT+15) stage are indicated. The horizontal red and yellow boxes indicate the periods of harvesting dry mature plants for physio-agronomical traits phenotyping.

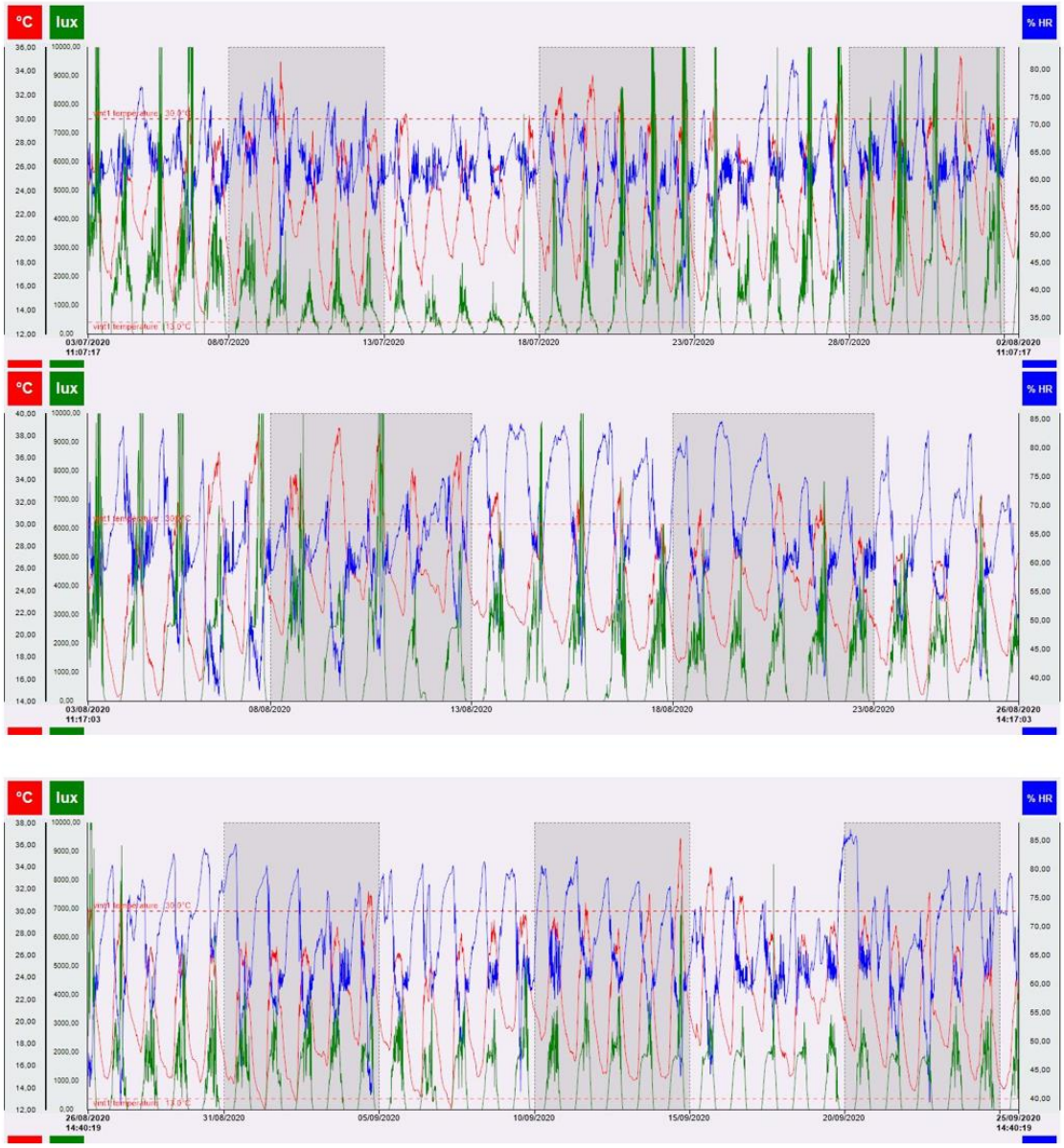


**Supplementary Figure 3: Meteorological data collected in the greenhouse for the 2020 experiment (Supplementary Figure 1).** In red the temperature in °C. In green the light intensity in Lux. In blue, the % of humidity. Data from July 3rd to September 26th 2020 are shown.

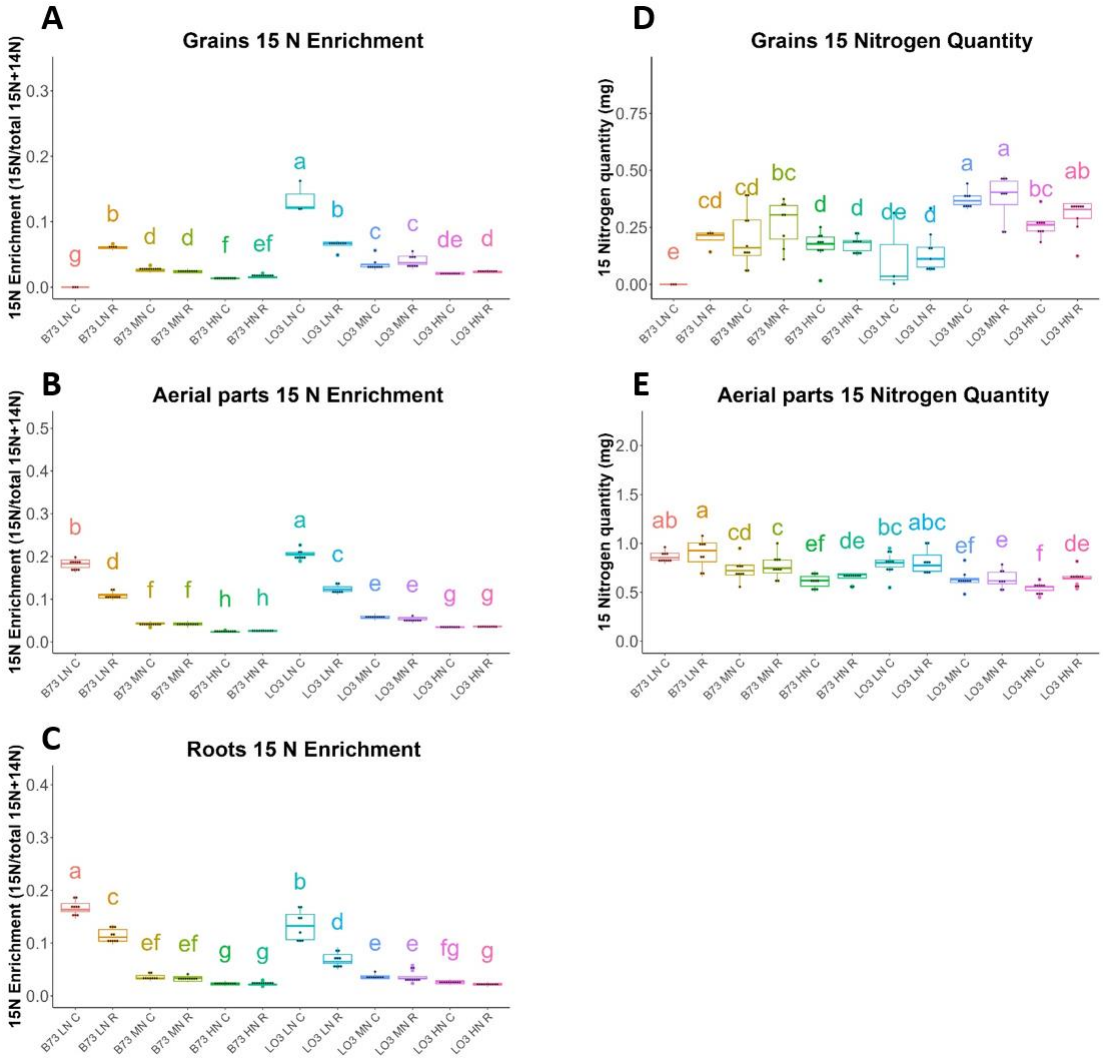


**Supplementary Figure 4: Impact of N supply on N isotope fractionation and N uptake efficiency in response to *R. irregularis* shows that AM symbiosis has a strong effect on N uptake efficiency en $^{15}$N enrichement.** Plants were subjected to a short pulse with a $^{15}$N labelled nutrient solution (See Materials and Methods)**. A, B** and **C :** $^{15}$N enrichment in grains, aerial parts and roots respectively. **D** and **E :** $^{15}$N quantity in mg in grains and aerial parts respectively. C: control, R: *R. irregularis* N=7-10 plants for grains and aerial parts. N=5 for roots. Different letters indicate significantly different averages for the considered trait by ANOVA.

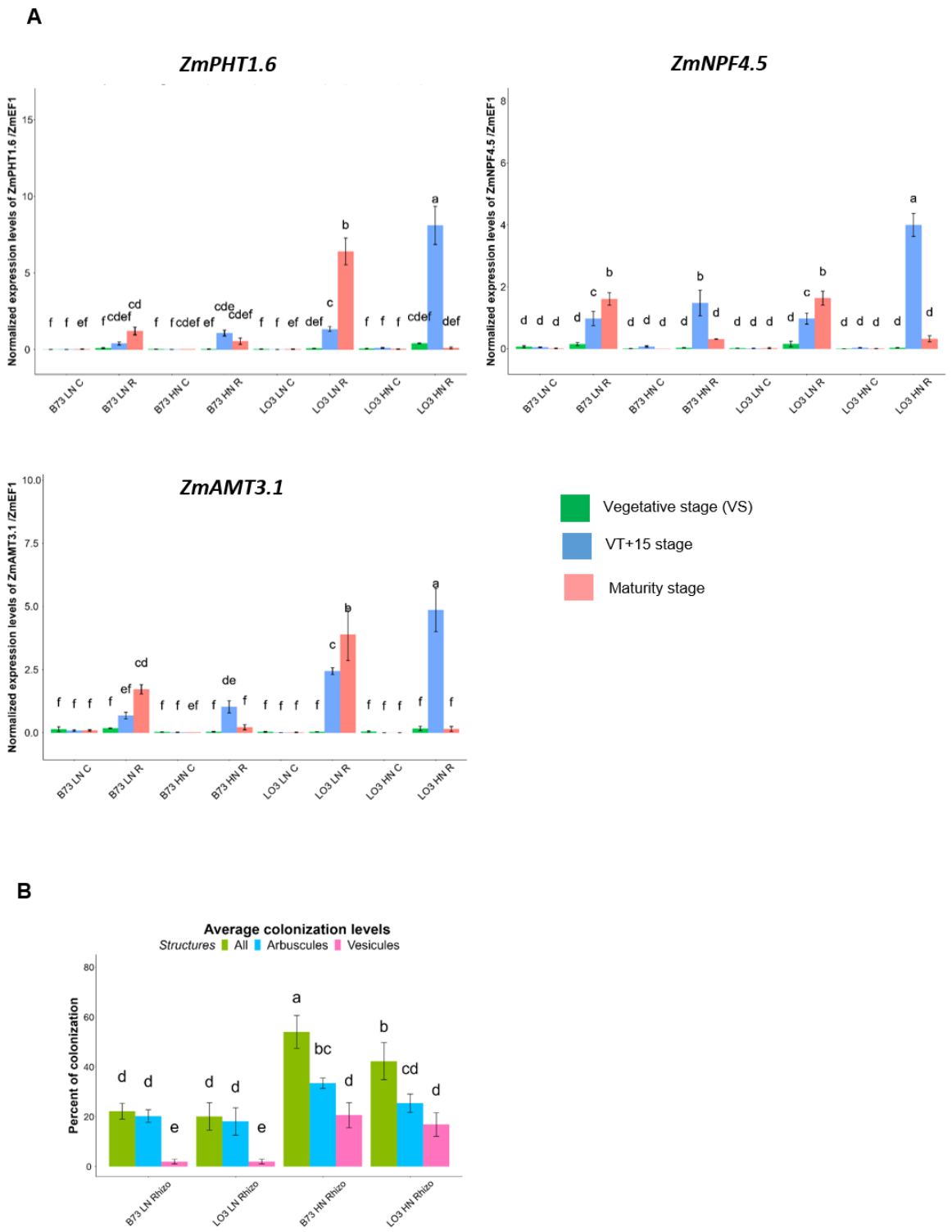


**Supplementary Figure 5 : Impact of N supply on *R. irregularis* colonization and kinetics of symbiosis marker gene expression. A**: AM Symbiostic gene expression levels quantified by qRT-PCR. **B**: Quantification of root colonization level by microscopic observation of different fungal structures (Struc) : arbuscules, vesicles and the sum of both (All) in roots harvested at VT+15 stage. C: control. R: *R. irregularis.* N=5. Bars indicate SD. Different letters indicate significantly different averages for the considered gene transcript level or trait by ANOVA.

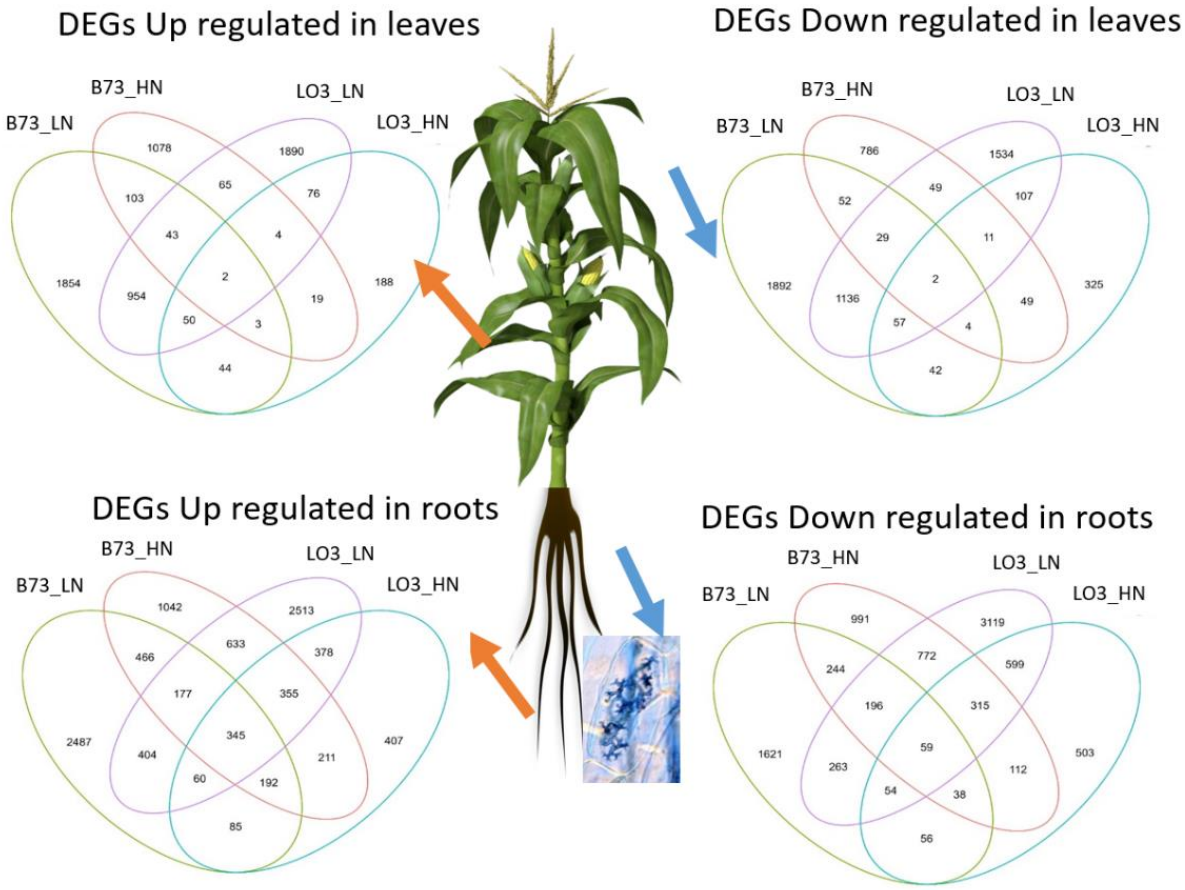


**Supplementary Figure 6 : Venn diagram of RNAseq data showing the overlap between maize DEG under LN or HN in line B73 and LO3.** Genes were selected so that their fold change (inoculated versus control) was > to 1.5 and statistically significant in the 3 replicates. B73_LN and B73_HN represent DEG genes up or down regulated in inoculated plants compared to control plants in LN or HN respectively; LO3_LN and LO3_HN represent DEG genes up or down regulated in inoculated plants compared to control plants in LN or HN respectively.

.

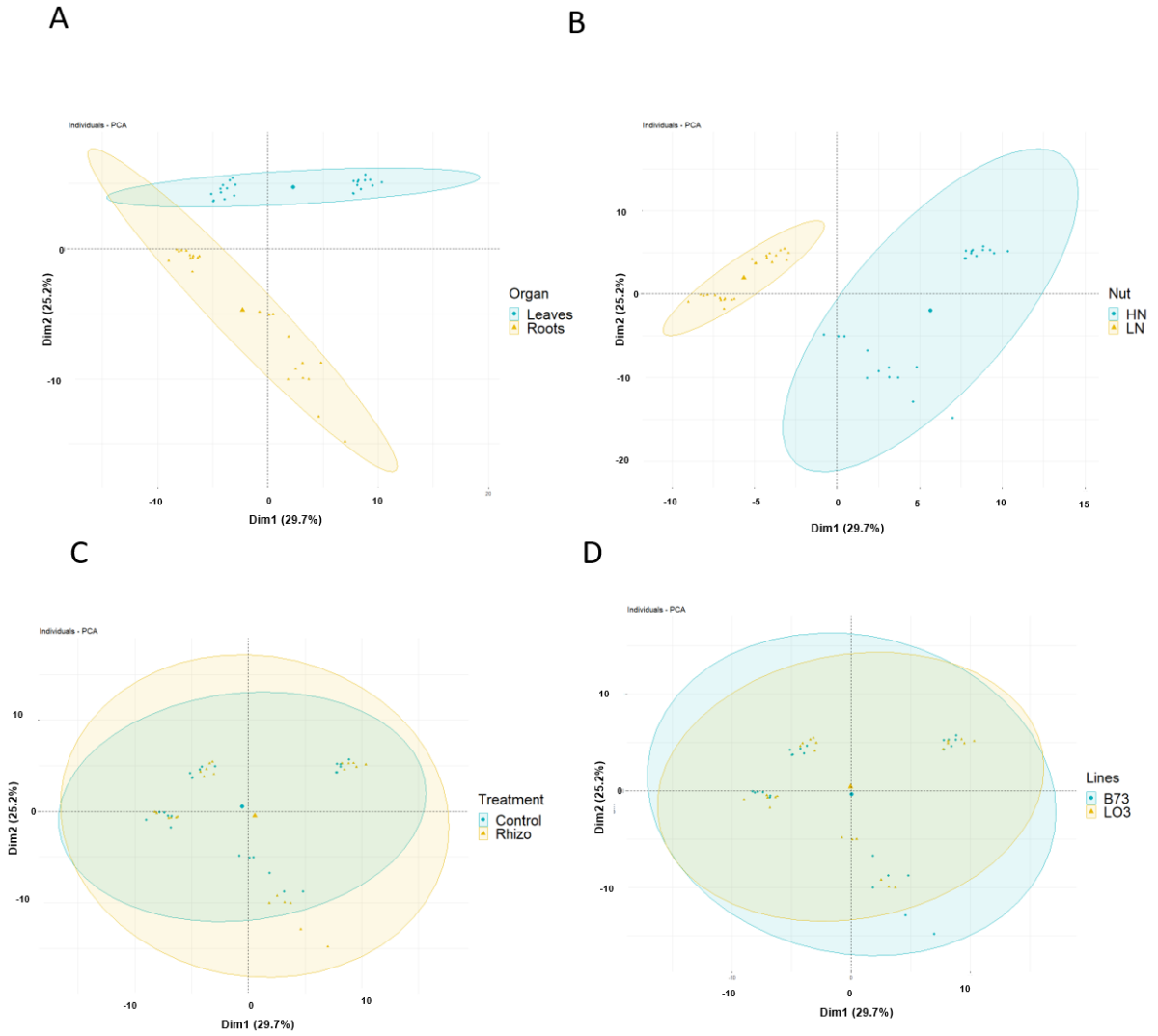


**Supplementary Figure 7: PCA on metabolomics data showing different impacts of N nutrition, organ, maize genotype or R. irregularis inoculation on metabolome**. Primary metabolite profiles were used to build these PCAs from leaves and roots of inoculated (RHIZO) or non-inoculated (Control) plants under LN or HN from B73 and Lo3 genotypes.

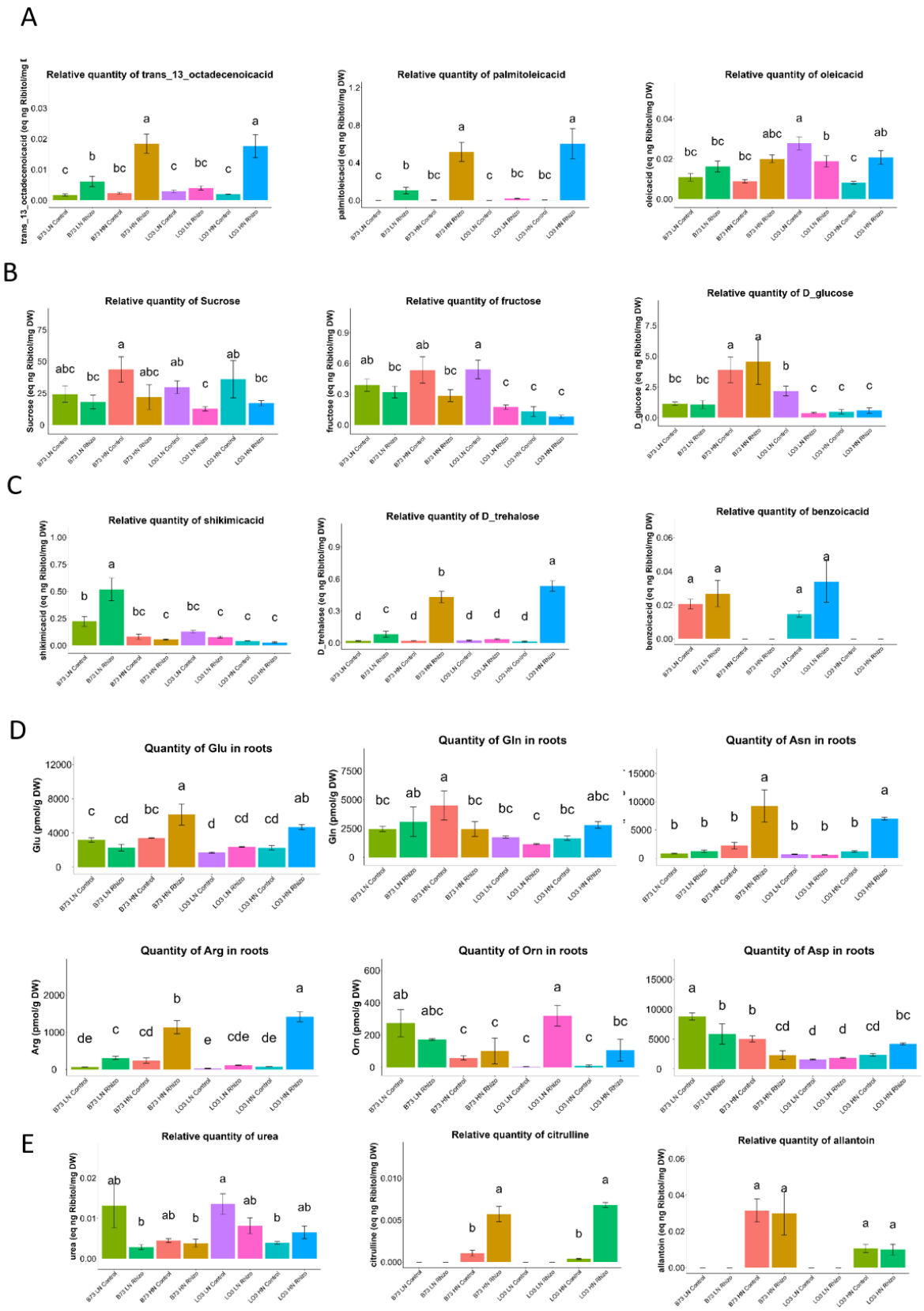


**Supplementary Figure 8 : Examples of metabolites accumulating in roots in response to R. irregularis.** Metabolites were quantified in identified samples by GS/MS in A, B,C and E or HPLC in D. **A**: examples of lipids. **B**: examples of soluble sugars. **C**: Examples of defense related metabolites. **D and E**: examples of N related metabolites.

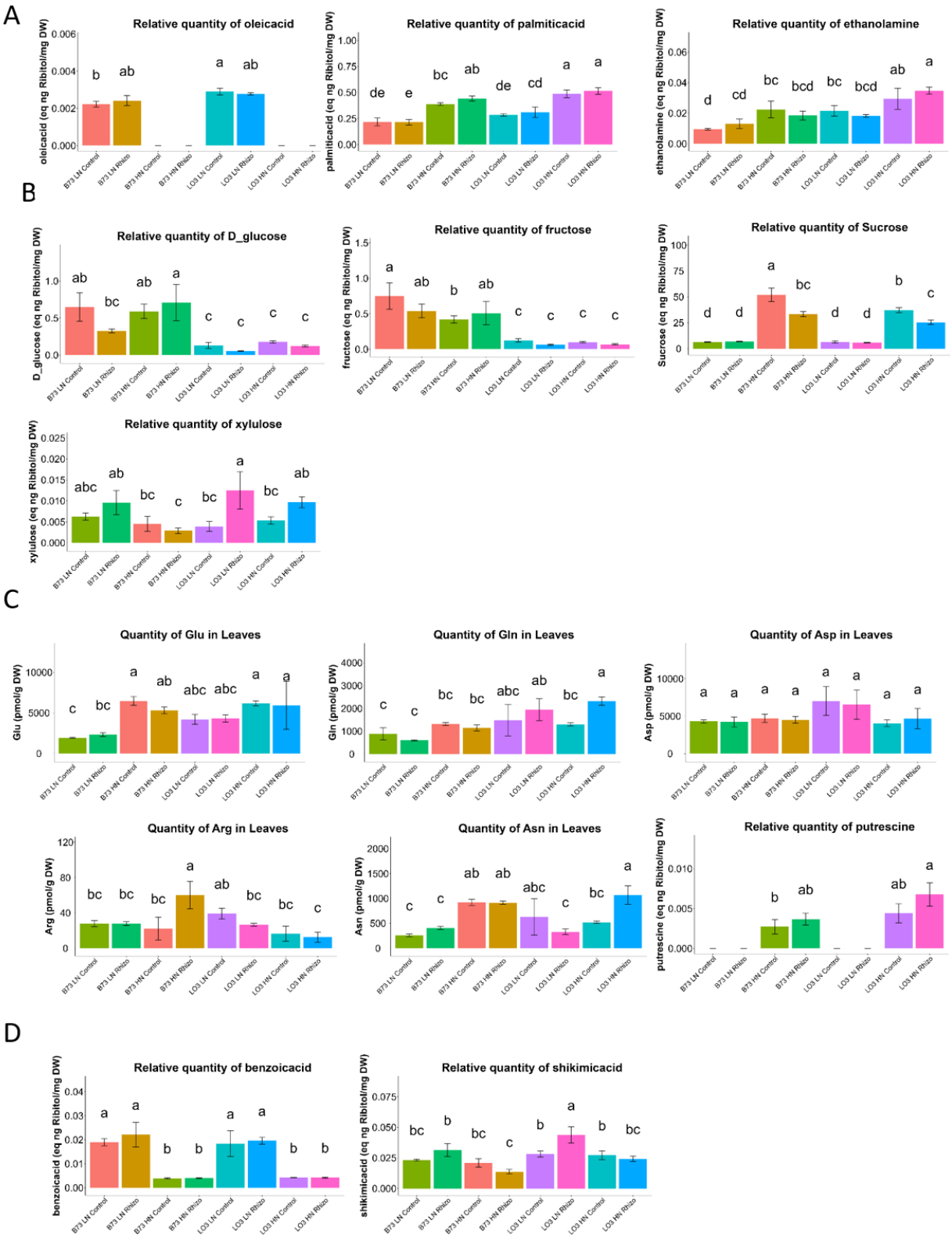


**Supplementary Figure 9 : Examples of metabolites accumulating in leaves in response to R. irregularis.** Metabolites were quantified in indicated samples by GS/MS or HPLC. Metabolites monitored by GC/MS are indicated by relative abundance to ribitol. Metabolites quantified by HPLC are indicated by absolute quantities (pmol/g DW). **A**: examples of lipid related metabolites. **B**: examples of sugars. **C**: Examples of N related metabolites. **D** : Examples of defense related metabolites.

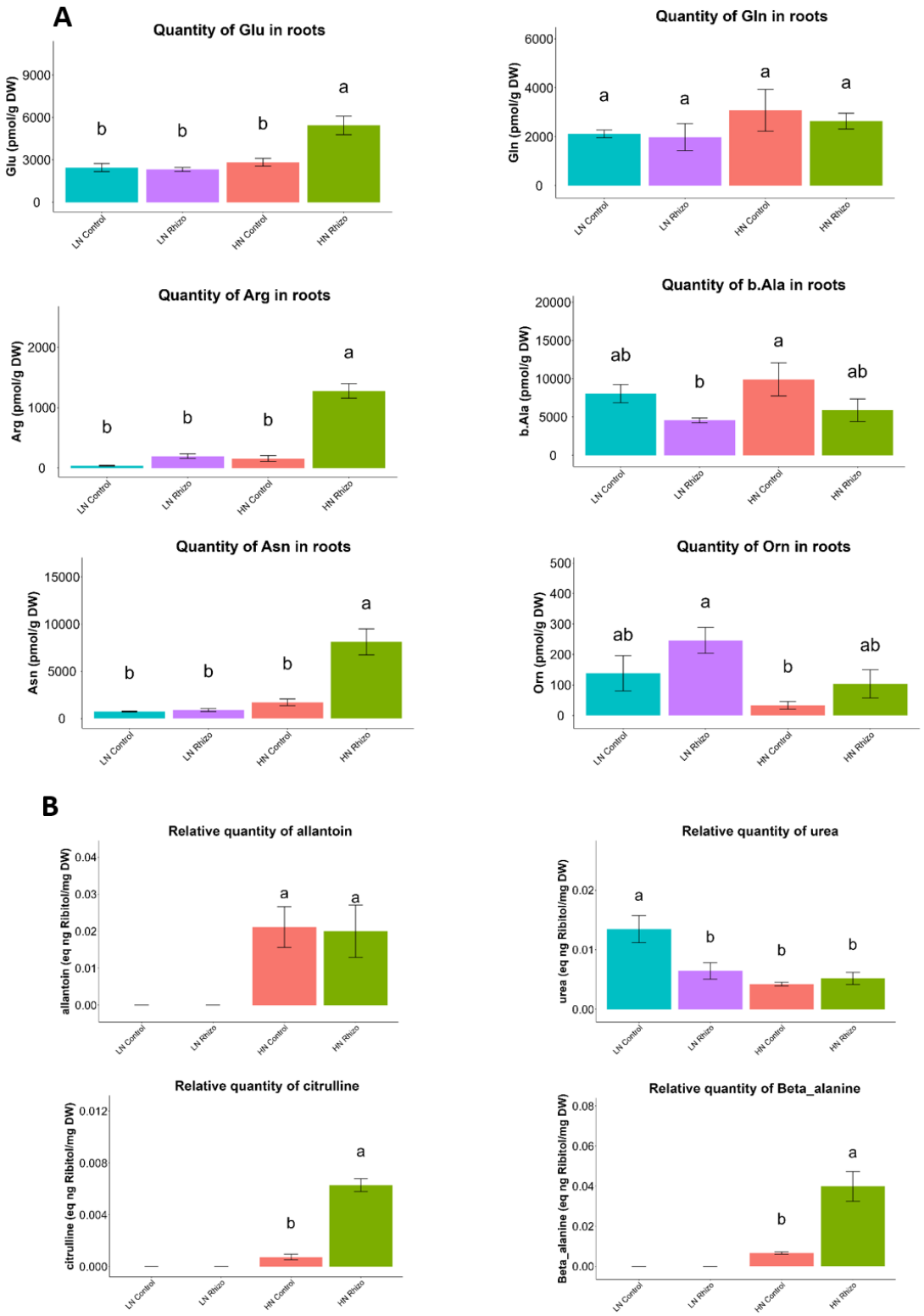


**Supplementary Figure 10 : Metabolite profiles supporting hypothetical model in roots.** Metabolites related to the transcrptomic data are represented. To build the model, the data from both B73 and Lo3 maize lines were pooled. Here we only considered the N nutriton effect. **A:** metabolites quantified by HPLC. In **B** metabolites monitored by GC/MS.

**References:**

**AU - Baudry K, AU - Paysant-Le Roux C, AU - Colella S, AU - Castandet B, AU - Martin M-L**. 2022. Analyzing Multifactorial RNA-Seq Experiments with DiCoExpress. JoVE, e62566.

**Bago B, Pfeffer P, Shachar-Hill Y**. 2001. Could the Urea Cycle Be Translocating Nitrogen in the Arbuscular Mycorrhizal Symbiosis? The New Phytologist **149**, 4–8.

**Balzergue C, Chabaud M, Barker D, Bécard G, Rochange S**. 2013. High phosphate reduces host ability to develop arbuscular mycorrhizal symbiosis without affecting root calcium spiking responses to the fungus . Frontiers in Plant Science **4**.

**Bar-Hen A, Barbillon P, Donnet S**. 2020. Block models for generalized multipartite networks: Applications in ecology and ethnobiology. Statistical Modelling **22**, 273–296.

**BARROSO J, CASIMIRO A, CARRAPIÇO F, SLOMÉ M, PAIS S**. 1988. Localization of uricase in mycorrhizas of Ophrys lutea Cav. New Phytologist **108**, 335–340.

**Berger F, Gutjahr C**. 2021. Factors affecting plant responsiveness to arbuscular mycorrhiza. Current Opinion in Plant Biology **59**, 101994.

**Breuillin F, Schramm J, Hajirezaei M, *et al.*** 2010. Phosphate systemically inhibits development of arbuscular mycorrhiza in Petunia hybrida and represses genes involved in mycorrhizal functioning. The Plant Journal **64**, 1002–1017.

Bushnell B (2014). BBMap: A Fast, Accurate, Splice-Aware Aligner. United States: N. p., 2014. sourceforge.net/projects/bbmap/

**Cañas RA, Yesbergenova-Cuny Z, Simons M, *et al.*** 2017. Exploiting the Genetic Diversity of Maize Using a Combined Metabolomic, Enzyme Activity Profiling, and Metabolic Modeling Approach to Link Leaf Physiology to Kernel Yield. The Plant Cell **29**, 919–943.

**Chen A, Gu M, Wang S, Chen J, Xu G**. 2018*a*. Transport properties and regulatory roles of nitrogen in arbuscular mycorrhizal symbiosis. Seminars in Cell & Developmental Biology **74**, 80–88.

**Chen ECH, Morin E, Beaudet D, *et al.*** 2018*b*. High intraspecific genome diversity in the model arbuscular mycorrhizal symbiont Rhizophagus irregularis. New Phytologist **220**, 1161–1171.

**Cheng C-Y, Li Y, Varala K, *et al.*** 2021. Evolutionarily informed machine learning enhances the power of predictive gene-to-phenotype relationships. Nature Communications **12**, 5627.

**Cho L-H, Yoon J, Tun W, *et al.*** 2022. Cytokinin increases vegetative growth period by suppressing florigen expression in rice and maize. The Plant Journal **110**, 1619–1635.

**Choi J, Summers W, Paszkowski U**. 2018. Mechanisms Underlying Establishment of Arbuscular Mycorrhizal Symbioses. Annual Review of Phytopathology **56**, 135–160.

**Chowdhury NB, Alsiyabi A, Saha R**. 2022*a*. Characterizing the Interplay of Rubisco and Nitrogenase Enzymes in Anaerobic-Photoheterotrophically Grown Rhodopseudomonas palustris CGA009 through a Genome-Scale Metabolic and Expression Model. Microbiology Spectrum **10**, e01463-22.

**Chowdhury NB, Decouard B, Quillere I, *et al.*** 2023. Multi-organ Metabolic Model of <em>Zea mays</em> Connects Temperature Stress with Thermodynamics-Reducing Power-Energy Generation Axis. bioRxiv, 2023.07.09.548275.

**Chowdhury NB, Schroeder WL, Sarkar D, Amiour N, Quilleré I, Hirel B, Maranas CD, Saha R**. 2022*b*. Dissecting the metabolic reprogramming of maize root under nitrogen-deficient stress conditions. Journal of Experimental Botany **73**, 275–291.

**Courty PE, Smith P, Koegel S, Redecker D, Wipf D**. 2015. Inorganic Nitrogen Uptake and Transport in Beneficial Plant Root-Microbe Interactions. Critical Reviews in Plant Sciences **34**, 4–16.

**Das D, Paries M, Hobecker K, Gigl M, Dawid C, Lam H-M, Zhang J, Chen M, Gutjahr C**. 2022. PHOSPHATE STARVATION RESPONSE transcription factors enable arbuscular mycorrhiza symbiosis. Nature Communications **13**, 477.

**Dechorgnat J, Francis KL, Dhugga KS, Rafalski JA, Tyerman SD, Kaiser BN**. 2019. Tissue

and nitrogen-linked expression profiles of ammonium and nitrate transporters in maize. BMC Plant Biology **19**, 206.

**Dellagi A, Quillere I, Hirel B**. 2020. Beneficial soil-borne bacteria and fungi: a promising way to improve plant nitrogen acquisition. Journal of Experimental Botany **71**, 4469–4479.

**Dobin A, Davis CA, Schlesinger F, Drenkow J, Zaleski C, Jha S, Batut P, Chaisson M, Gingeras TR**. 2013. STAR: ultrafast universal RNA-seq aligner. Bioinformatics **29**, 15–21.

**Fan X, Naz M, Fan X, Xuan W, Miller AJ, Xu G**. 2017. Plant nitrate transporters: from gene function to application. Journal of Experimental Botany **68**, 2463–2475.

**Fernie AR, Bachem CWB, Helariutta Y, *et al.*** 2020. Synchronization of developmental, molecular and metabolic aspects of source–sink interactions. Nature Plants **6**, 55–66.

**Fiehn O**. 2006. Metabolite Profiling in Arabidopsis BT - Arabidopsis Protocols. In: Salinas J,, In: Sanchez-Serrano JJ, eds. Totowa, NJ: Humana Press, 439–447.

**Fiehn O, Wohlgemuth G, Scholz M, Kind T, Lee DY, Lu Y, Moon S, Nikolau B**. 2008. Quality control for plant metabolomics: reporting MSI-compliant studies. The Plant Journal **53**, 691–704.

**Fiorilli V, Catoni M, Miozzi L, Novero M, Accotto GP, Lanfranco L**. 2009. Global and cell-type gene expression profiles in tomato plants colonized by an arbuscular mycorrhizal fungus. New Phytologist **184**, 975–987.

**Gagnot S, Tamby J-P, Martin-Magniette M-L, Bitton F, Taconnat L, Balzergue S, Aubourg S, Renou J-P, Lecharny A, Brunaud V**. 2008. CATdb: a public access to Arabidopsis transcriptome data from the URGV-CATMA platform. Nucleic Acids Research **36**, D986–D990.

**Galili T, O'Callaghan A, Sidi J, Sievert C**. 2018. heatmaply: an R package for creating interactive cluster heatmaps for online publishing. Bioinformatics **34**, 1600–1602.

**Gallou A, Declerck S, Cranenbrouck S**. 2012. Transcriptional regulation of defence genes and involvement of the WRKY transcription factor in arbuscular mycorrhizal potato root

colonization. Functional & Integrative Genomics **12**, 183–198.

**Garcia K, Doidy J, Zimmermann SD, Wipf D, Courty P-E**. 2016. Take a Trip Through the Plant and Fungal Transportome of Mycorrhiza. Trends in Plant Science **21**, 937–950.

**Gianinazzi S, Gollotte A, Binet M-N, van Tuinen D, Redecker D, Wipf D**. 2010. Agroecology: the key role of arbuscular mycorrhizas in ecosystem services. Mycorrhiza **20**, 519–530.

**Giovannetti M, Mosse B**. 1980. An Evaluation of Techniques for Measuring Vesicular Arbuscular Mycorrhizal Infection in Roots. The New Phytologist **84**, 489–500.

**Gojon A**. 2022. Nitrogen acquisition in arbuscular mycorrhizal symbioses: A step into the real world. Journal of Plant Physiology **271**, 153646.

**Grandclaudon M, Perrot-Dockès M, Trichot C, *et al.*** 2019. A Quantitative Multivariate Model of Human Dendritic Cell-T Helper Cell Communication. Cell **179**, 432-447.e21.

**Handa Y, Nishide H, Takeda N, Suzuki Y, Kawaguchi M, Saito K**. 2015. RNA-seq Transcriptional Profiling of an Arbuscular Mycorrhiza Provides Insights into Regulated and Coordinated Gene Expression in Lotus japonicus and Rhizophagus irregularis. Plant and Cell Physiology **56**, 1490–1511.

**Hirel B, Le Gouis J, Ney B, Gallais A**. 2007. The challenge of improving nitrogen use efficiency in crop plants: Towards a more central role for genetic variability and quantitative genetics within integrated approaches. Journal of Experimental Botany.

**Hirel B, Krapp ABT-RM in LS**. 2020. Nitrogen Utilization in Plants I Biological and Agronomic Importance. Elsevier, .

**Hirel B, Tétu T, Lea PJ, Dubois F**. 2011. Improving Nitrogen Use Efficiency in Crops for Sustainable Agriculture. Sustainability **3**.

**Hui J, An X, Li Z, *et al.*** 2022. The mycorrhiza-specific ammonium transporter ZmAMT3;1 mediates mycorrhiza-dependent nitrogen uptake in maize roots. The Plant Cell **34**, 4066–

4087.

**Hull R, Choi J, Paszkowski U**. 2021. Conditioning plants for arbuscular mycorrhizal symbiosis through DWARF14-LIKE signalling. Current Opinion in Plant Biology **62**, 102071.

**Ingraffia R, Amato G, Sosa-Hernández MA, Frenda AS, Rillig MC, Giambalvo D**. 2020. Nitrogen Type and Availability Drive Mycorrhizal Effects on Wheat Performance, Nitrogen Uptake and Recovery, and Production Sustainability . Frontiers in Plant Science **11**, 760.

**Kant S**. 2018. Understanding nitrate uptake, signaling and remobilisation for improving plant nitrogen use efficiency. Seminars in Cell & Developmental Biology **74**, 89–96.

**Kaur S, Suseela V**. 2020. Unraveling Arbuscular Mycorrhiza-Induced Changes in Plant Primary and Secondary Metabolome. Metabolites **10**.

**Keymer A, Pimprikar P, Wewer V, *et al.*** 2017. Lipid transfer from plants to arbuscular mycorrhiza fungi (G Stacey, Ed.). eLife **6**, e29107.

**Kopylova E, Noé L, Touzet H**. 2012. SortMeRNA: fast and accurate filtering of ribosomal RNAs in metatranscriptomic data. Bioinformatics **28**, 3211–3217.

**Krapp A, David LC, Chardin C, Girin T, Marmagne A, Leprince AS, Chaillou S, Ferrario-Méry S, Meyer C, Daniel-Vedele F**. 2014. Nitrate transport and signalling in Arabidopsis. Journal of Experimental Botany.

**Lambert I, Paysant-Le Roux C, Colella S, Martin-Magniette M-L**. 2020. DiCoExpress: a tool to process multifactorial RNAseq experiments from quality controls to co-expression analysis through differential analysis based on contrasts inside GLM models. Plant Methods **16**, 68.

**Lanfranco L, Fiorilli V, Gutjahr C**. 2018. Partner communication and role of nutrients in the arbuscular mycorrhizal symbiosis. New Phytologist **220**, 1031–1046.

**Lassaletta L, Billen G, Garnier J, Bouwman L, Velazquez E, Mueller ND, Gerber JS**. 2016. Nitrogen use in the global food system: past trends and future trajectories of agronomic performance, pollution, trade, and dietary demand. Environmental Research Letters **11**,

095007.

**Lea PJ, Miflin BJ**. 2018. Nitrogen Assimilation and its Relevance to Crop Improvement. Annual Plant Reviews online, 1–40.

**Lee D-K, Redillas MCFR, Jung H, Choi S, Kim YS, Kim J-K**. 2018. A Nitrogen Molecular Sensing System, Comprised of the ALLANTOINASE and UREIDE PERMEASE 1 Genes, Can Be Used to Monitor N Status in Rice . Frontiers in Plant Science **9**.

**Li F, Chung T, Pennington JG, Federico ML, Kaeppler HF, Kaeppler SM, Otegui MS, Vierstra RD**. 2015. Autophagic Recycling Plays a Central Role in Maize Nitrogen Remobilization. The Plant Cell **27**, 1389–1408.

**Liu J, Fernie AR, Yan J**. 2020. The Past, Present, and Future of Maize Improvement: Domestication, Genomics, and Functional Genomic Routes toward Crop Enhancement. Plant Communications **1**, 100010.

**Liu Q, Wu K, Song W, Zhong N, Wu Y, Fu X**. 2022. Improving Crop Nitrogen Use Efficiency Toward Sustainable Green Revolution. Annual Review of Plant Biology **73**, 523–551.

**MacLean AM, Bravo A, Harrison MJ**. 2017. Plant Signaling and Metabolic Pathways Enabling Arbuscular Mycorrhizal Symbiosis. The Plant Cell **29**, 2319–2335.

**Masclaux-Daubresse C, Daniel-Vedele F, Dechorgnat J, Chardon F, Gaufichon L, Suzuki A**. 2010. Nitrogen uptake, assimilation and remobilization in plants: Challenges for sustainable and productive agriculture. Annals of Botany.

**Masson-Boivin C, Sachs JL**. 2018. Symbiotic nitrogen fixation by rhizobia—the roots of a success story. Current Opinion in Plant Biology **44**, 7–15.

**Mateus ID, Masclaux FG, Aletti C, Rojas EC, Savary R, Dupuis C, Sanders IR**. 2019. Dual RNA-seq reveals large-scale non-conserved genotype × genotype-specific genetic reprograming and molecular crosstalk in the mycorrhizal symbiosis. The ISME Journal **13**, 1226–1238.

**McCarthy DJ, Chen Y, Smyth GK**. 2012. Differential expression analysis of multifactor RNA-Seq experiments with respect to biological variation. Nucleic Acids Research **40**, 4288–4297.

**Melino VJ, Tester MA, Okamoto M**. 2022. Strategies for engineering improved nitrogen use efficiency in crop plants via redistribution and recycling of organic nitrogen. Current Opinion in Biotechnology **73**, 263–269.

**Menadue DJ, Riboni M, Baumann U, Schilling RK, Plett DC, Roy SJ**. 2021. Proton-pumping pyrophosphatase homeolog expression is a dynamic trait in bread wheat (Triticum aestivum). Plant Direct **5**, e354.

**Meng L, Zhang A, Wang F, Han X, Wang D, Li S**. 2015. Arbuscular mycorrhizal fungi and rhizobium facilitate nitrogen uptake and transfer in soybean/maize intercropping system . Frontiers in Plant Science **6**.

**Morris DS, Chowdhury NB, Kathol M, Saha R**. 2023. Opening the door to nitrogen fixation in oxygenic phototrophs. Trends in Biotechnology **41**, 283–285.

**Murphy J, Riley JP**. 1962. A modified single solution method for the determination of phosphate in natural waters. Analytica Chimica Acta **27**, 31–36.

**Murtagh F, Legendre P**. 2014. Ward's Hierarchical Agglomerative Clustering Method: Which Algorithms Implement Ward's Criterion? Journal of Classification **31**, 274–295.

**Nanjareddy K, Arthikala M-K, Gómez B-M, Blanco L, Lara M**. 2017. Differentially expressed genes in mycorrhized and nodulated roots of common bean are associated with defense, cell wall architecture, N metabolism, and P metabolism. PLOS ONE **12**, e0182328.

**Paries M, Gutjahr C**. 2023. The good, the bad, and the phosphate: regulation of beneficial and detrimental plant–microbe interactions by the plant phosphate status. New Phytologist **239**, 29–46.

**Perrot-Dockès M, Lévy-Leduc C, Rajjou L**. 2022. Estimation of Large Block Structured Covariance Matrices: Application to 'Multi-Omic' Approaches to Study Seed Quality. Journal

of the Royal Statistical Society Series C: Applied Statistics **71**, 119–147.

**Perrot-Dockès M, Lévy-Leduc C, Sansonnet L, Chiquet J**. 2018. Variable selection in multivariate linear models with high-dimensional covariance matrix estimation. Journal of Multivariate Analysis **166**, 78–97.

**Plassard C, Becquer A, Garcia K**. 2019. Phosphorus Transport in Mycorrhiza: How Far Are We? Trends in Plant Science **24**, 794–801.

**Prioul J-L, Schwebel-Dugué N**. 1992. Source-Sink Manipulations and Carbohydrate Metabolism in Maize. Crop Science **32**, cropsci1992.0011183X003200030035x.

**Quiroga G, Erice G, Aroca R, Delgado-Huertas A, Ruiz-Lozano JM**. 2020. Elucidating the Possible Involvement of Maize Aquaporins and Arbuscular Mycorrhizal Symbiosis in the Plant Ammonium and Urea Transport under Drought Stress Conditions. Plants **9**.

**Ramírez-Flores MR, Bello-Bello E, Rellán-Álvarez R, Sawers RJH, Olalde-Portugal V**. 2019. Inoculation with the mycorrhizal fungus Rhizophagus irregularis modulates the relationship between root growth and nutrient content in maize (Zea mays ssp. mays L.). Plant Direct **3**, e00192.

**Ranum P, Peña-Rosas JP, Garcia-Casal MN**. 2014. Global maize production, utilization, and consumption. Annals of the New York Academy of Sciences **1312**, 105–112.

**Revilla P, Alves ML, Andelković V, *et al.*** 2022. Traditional Foods From Maize (Zea mays L.) in Europe . Frontiers in Nutrition **8**.

**Rigaill G, Balzergue S, Brunaud V, *et al.*** 2018. Synthetic data sets for the identification of key ingredients for RNA-seq differential analysis. Briefings in Bioinformatics **19**, 65–76.

**Robinson MD, McCarthy DJ, Smyth GK**. 2010. edgeR: a Bioconductor package for differential expression analysis of digital gene expression data. Bioinformatics **26**, 139–140.

**Sakakibara H, Takei K, Hirose N**. 2006. Interactions between nitrogen and cytokinin in the regulation of metabolism and development. Trends in Plant Science.

**Sawers RJH, Ramírez-Flores MR, Olalde-Portugal V, Paszkowski U**. 2018*a*. The impact of domestication and crop improvement on arbuscular mycorrhizal symbiosis in cereals: insights from genetics and genomics. New Phytologist **220**, 1135–1140.

**Sawers RJHH, Ramírez-Flores MR, Olalde-Portugal V, Paszkowski U**. 2018*b*. The impact of domestication and crop improvement on arbuscular mycorrhizal symbiosis in cereals: insights from genetics and genomics. New Phytologist **220**, 1135–1140.

**Sawers RJH, Svane SF, Quan C, *et al.*** 2017. Phosphorus acquisition efficiency in arbuscular mycorrhizal maize is correlated with the abundance of root-external hyphae and the accumulation of transcripts encoding PHT1 phosphate transporters. New Phytologist **214**, 632–643.

**Schaarschmidt S, Gresshoff PM, Hause B**. 2013. Analyzing the soybean transcriptome during autoregulation of mycorrhization identifies the transcription factors GmNF-YA1a/b as positive regulators of arbuscular mycorrhization. Genome Biology **14**, R62.

**Schlesinger WH**. 2009. On the fate of anthropogenic nitrogen. Proceedings of the National Academy of Sciences **106**, 203 LP – 208.

**Schmidt JE, Bowles TM, Gaudin ACM**. 2016. Using Ancient Traits to Convert Soil Health into Crop Yield: Impact of Selection on Maize Root and Rhizosphere Function . Frontiers in Plant Science **7**.

**Schnable PS, Ware D, Fulton RS, *et al.*** 2009. The B73 Maize Genome: Complexity, Diversity, and Dynamics. Science **326**, 1112–1115.

**Simons M, Saha R, Guillard L, Clément G, Armengaud P, Cañas R, Maranas CD, Lea PJ, Hirel B**. 2014. Nitrogen-use efficiency in maize (Zea mays L.): From ‘omics’ studies to metabolic modelling. Journal of Experimental Botany **65**, 5657–5671.

**Smith SE, Jakobsen I, Grønlund M, Smith FA**. 2011. Roles of Arbuscular Mycorrhizas in Plant Phosphorus Nutrition: Interactions between Pathways of Phosphorus Uptake in

Arbuscular Mycorrhizal Roots Have Important Implications for Understanding and Manipulating Plant Phosphorus Acquisition. Plant Physiology **156**, 1050–1057.

**Smith SE, Read DJ**. 2002. Mineral nutrition, heavy metal accumulation and water relations of VA mycorrhizal plants. Mycorrhizal Symbiosis, 126–160.

**Su H, Cao Y, Ku L, *et al.*** 2018. Dual functions of ZmNF-YA3 in photoperiod-dependent flowering and abiotic stress responses in maize. Journal of Experimental Botany **69**, 5177–5189.

**Tegeder M**. 2014. Transporters involved in source to sink partitioning of amino acids and ureides: opportunities for crop improvement. Journal of Experimental Botany **65**, 1865–1878.

**Thakur K, Garg N**. 2023. Differential Role of Silicon and Rhizoglomus intraradices in Modulating Amide and Ureide Metabolism of Seasonally Different Legume Species Subjected to Nickel Toxicity. Silicon.

**Tisserant E, Malbreil M, Kuo A, *et al.*** 2013. Genome of an arbuscular mycorrhizal fungus provides insight into the oldest plant symbiosis. Proceedings of the National Academy of Sciences **110**, 20117–20122.

**Tóth K, Stacey G**. 2015. Does plant immunity play a critical role during initiation of the legume-rhizobium symbiosis? . Frontiers in Plant Science **6**.

**Udvardi M, Poole PS**. 2013. Transport and Metabolism in Legume-Rhizobia Symbioses. Annual Review of Plant Biology **64**, 781–805.

**Urrutia M, Blein-Nicolas M, Fernandez O, Bernillon S, Maucourt M, Deborde C, Balliau T, Rabier D, Bénard C, Prigent S**. 2023. Identification of metabolic and protein markers representative of the impact of mild nitrogen deficit on agronomic performance of maize hybrids.

**Vangelisti A, Natali L, Bernardi R, Sbrana C, Turrini A, Hassani-Pak K, Hughes D, Cavallini A, Giovannetti M, Giordani T**. 2018. Transcriptome changes induced by arbuscular

mycorrhizal fungi in sunflower (Helianthus annuus L.) roots. Scientific Reports **8**, 4.

**Verly C, Djoman ACR, Rigault M, Giraud F, Rajjou L, Saint-Macary ME, Dellagi A**. 2020. Plant Defense Stimulator Mediated Defense Activation Is Affected by Nitrate Fertilization and Developmental Stage in Arabidopsis thaliana. Frontiers in Plant Science.

**Verzeaux J, Hirel B, Dubois F, Lea PJ, Tétu T**. 2017. Agricultural practices to improve nitrogen use efficiency through the use of arbuscular mycorrhizae: Basic and agronomic aspects. Plant Science **264**, 48–56.

**Wang S, Chen A, Xie K, *et al.*** 2020. Functional analysis of the OsNPF4.5 nitrate transporter reveals a conserved mycorrhizal pathway of nitrogen acquisition in plants. Proceedings of the National Academy of Sciences **117**, 16649 LP – 16659.

**Wang Y-Y, Cheng Y-H, Chen K-E, Tsay Y-F**. 2018. Nitrate Transport, Signaling, and Use Efficiency. Annual Review of Plant Biology **69**, 85–122.

**Wang W, Shi J, Xie Q, Jiang Y, Yu N, Wang E**. 2017. Nutrient Exchange and Regulation in Arbuscular Mycorrhizal Symbiosis. Molecular Plant **10**, 1147–1158.

**Wang E, Yu N, Bano SA, *et al.*** 2014. A H+-ATPase That Energizes Nutrient Uptake during Mycorrhizal Symbioses in Rice and Medicago truncatula . The Plant Cell **26**, 1818–1830.

**Wani SH, Vijayan R, Choudhary M, Kumar A, Zaid A, Singh V, Kumar P, Yasin JK**. 2021. Nitrogen use efficiency (NUE): elucidated mechanisms, mapped genes and gene networks in maize (Zea mays L.). Physiology and Molecular Biology of Plants **27**, 2875–2891.

**Wipf D, Krajinski F, van Tuinen D, Recorbet G, Courty P-E**. 2019. Trading on the arbuscular mycorrhiza market: from arbuscules to common mycorrhizal networks. New Phytologist **223**, 1127–1142.

**Witte CP, Herde M**. 2020*a*. Nucleotide metabolism in plants. Plant Physiology **182**, 63–78.

**Witte C-P, Herde M**. 2020*b*. Nucleotide Metabolism in Plants1 [OPEN]. Plant Physiology **182**, 63–78.

**Xie K, Ren Y, Chen A, Yang C, Zheng Q, Chen J, Wang D, Li Y, Hu S, Xu G**. 2022. Plant nitrogen nutrition: The roles of arbuscular mycorrhizal fungi. Journal of Plant Physiology **269**, 153591.

**Yonekura-Sakakibara K, Kojima M, Yamaya T, Sakakibara H**. 2004. Molecular Characterization of Cytokinin-Responsive Histidine Kinases in Maize. Differential Ligand Preferences and Response to cis-Zeatin. Plant Physiology **134**, 1654–1661.

**Yooyongwech S, Threeprom W, Tisarum R, Samphumphuang T, Chungloo D, Cha-um S**. 2022. Matching of Nitrogen Enhancement and Photosynthetic Efficiency by Arbuscular Mycorrhiza in Maize (Zea mays L.) in Relation to Organic Fertilizer Type. Plants **11**.

**Yu X, Keitel C, Zhang Y, Wangeci AN, Dijkstra FA**. 2022. Global meta-analysis of nitrogen fertilizer use efficiency in rice, wheat and maize. Agriculture, Ecosystems and Environment **338**, 108089.

**Zrenner R, Stitt M, Sonnewald U, Boldt R**. 2006. PYRIMIDINE AND PURINE BIOSYNTHESIS AND DEGRADATION IN PLANTS. Annual Review of Plant Biology **57**, 805–836.